International Journal of Solids and Structures xxx (2013) xxx–xxx

Contents lists available at SciVerse ScienceDirect

International Journal of Solids and Structures

journal homepage: www.elsevier.com/locate/ijsolstr

Micromechanical modeling of coupled viscoelastic–viscoplastic composites based on an incrementally affine formulation

B. Miled *, I. Doghri, L. Brassart, L. Delannay

Université catholique de Louvain (UCL), IMMC, Bâtiment Euler, 4 Avenue G. Lemaître, B-1348 Louvain-la-Neuve, Belgium

ARTICLE INFO

Article history:
Received 21 February 2012
Received in revised form 14 November 2012
Available online xxxx

Keywords:
Homogenization
Viscoelasticity
Viscoplasticity
Linearization
Numerical algorithms
Micromechanics

ABSTRACT

This study proposes a micromechanical modeling of inclusion-reinforced viscoelastic–viscoplastic composites, based on mean-field approaches. For this, we have generalized the so-called incrementally affine linearization method which was proposed by Doghri et al. (2010a) for elasto-viscoplastic materials. The proposal provides an affine relation between stress and strain increments via an algorithmic tangent operator. In order to find the incrementally affine expression, we start by the linearization of evolution equations at the beginning of a time step around the end time of the step. Next, a numerical integration of the linearized equations is required using a fully implicit backward Euler scheme. The obtained algebraic equations lead to an incrementally affine formulation which is form-similar to linear thermoelasticity, therefore known homogenization models for linear thermoelastic composites can be applied. The proposed method can deal with general viscoelastic–viscoplastic constitutive models with an arbitrary number of internal variables. The semi-analytical predictions are validated against finite element simulations and experimental results.

1. Introduction

Many materials including thermoplastic polymers (Polycarbonate, Polyamide, high density polyethylene, etc.), exhibit a rate-dependent behavior at all stages of deformation. The stress–strain response depends on the strain rate both below and above the yield stress. Upon unloading, the slope is rate-dependent and may be non-linear, even strongly so. Unloading to zero stress leads to a residual strain which decreases with time but does not disappear completely even after a long waiting period. All those features can be described by *coupled* viscoelastic–viscoplastic (VE–VP) constitutive models. This paper is concerned with the prediction of the effective properties of inclusion-reinforced VE–VP composites. Such materials are commonly used in a variety of engineering applications including automotive or aerospace industry.

A micro-mechanical approach is adopted, according to which the macroscopic stress–strain relation is computed based on an analysis at the level of individual constituents. Among methods of this kind one may cite: direct finite element (FE) analysis on representative cells of the microstructure, the asymptotic or mathematical theory of homogenization, the method of cells and subcells (which is related with the transformation field analysis), and mean-field homogenization (MFH) techniques. This work focuses on the latter method, which is based on assumed interaction laws between constitutive phases. Such models provide (hopefully reliable) estimates of the effective stress–strain relation, as well as a description of mechanical fields within the phases in terms of volume averages. The major advantage of MFH is its low computational cost, which makes it suitable for two-scale simulations of composite parts and structures.

Mean-field methods were first proposed for composites having linear elastic constituents. Most of them rely on the exact solution of Eshelby (1957) for an ellipsoidal inclusion embedded in an infinite matrix, like the (Mori and Tanaka, 1973), self-consistent (Hershey, 1954; Kröner, 1958; Hill, 1965) and double inclusion (Nemat-Nasser and Hori, 1999) schemes. Extension of these schemes to linear thermo-elasticity may be found in Camacho et al. (1990), Lielens (1999), Pierard et al. (2004), among others.

Extending these schemes to the nonlinear regime usually relies on the linearization of the local constitutive equations and the definition of uniform reference properties for each phase, valid for a given stage of deformation. Then, the homogenization problem becomes form-similar to an elastic or a thermo-elastic one, depending on the chosen linearization procedure. Popular linearization strategies include secant (Berveiller and Zaoui, 1979; Tandon and Weng, 1988), incremental (Hill, 1965), tangent (Molinari et al., 1987) and affine (Masson et al., 2000) approaches. The secant formulation uses the secant stiffness tensor to relate total stress and strain tensors, and is only valid for monotonic and proportional loading. The incremental formulation of Hill relates stress and

* Corresponding author. Current address: Centre des matériaux, UMR CNRS 7633, Ecole des mines de Paris, France. Tel.: +33 666 347 696.
E-mail address: miled.bilel@gmail.com (B. Miled).

0020-7683/$ - see front matter © 2013 Elsevier Ltd. All rights reserved.
http://dx.doi.org/10.1016/j.ijsolstr.2013.02.004

strain rates via an instantaneous tangent operator, and was initially developed for rate independent plasticity and later extended by Hutchinson (1976) who proposed a self-consistent homogenization for rigid viscoplastic polycrystals.

An alternative treatment of viscoplasticity was proposed by Weng (1982), who extended the formulation of Kröner (1961). In this approach, the plastic strain (rate) is considered as an eigenstrain (stress-free strain) in the isolated inclusion representation of Eshelby. Consequently, mechanical interactions among the phases are treated in a purely elastic way, leading to overstiff predictions of the overall behavior. The idea was extended to finite strains by Nemat-Nasser and Obata (1986), but was also shown to yield too stiff predictions (Molinari et al., 1997). It also sustains mean-field models derived from the transformation field analysis (Dvorak, 1992; Chaboche et al., 2001).

Homogenization of viscoelastic composites is usually performed invoking the correspondence principle (Friebel et al., 2006; Hashin, 1965; Hashin, 1970; Laws and McLaughlin, 1978), according to which constitutive equations in the time domain can be recast into a linear elastic form into the Laplace domain. After homogenization in the Laplace space, the effective properties in the time domain are found by the inverse transform. Extension to nonlinear viscoelasticity is achieved by linearizing the viscosity function, yielding successively a thermo-viscoelastic comparison composite in the time domain, and a linear thermoelastic fictitious composite in the Laplace domain. This approach was used to model elasto-viscoplastic composites by Masson and Zaoui (1999), and enhanced to fully account for internal variables by Pierard and Doghri (2006a), see also (Pierard, 2006; Pierard et al., 2007a). The main drawback of this approach is its numerical cost, related to the inversion of the Laplace transform.

Recently, several approaches were proposed to homogenize elasto-viscoplastic composites without recourse to Laplace transform. Molinari et al. (1997) and Molinari (2002) proposed an interaction law from the approximate solution of Eshelby's problem for an elasto-viscoplastic inclusion embedded into a matrix with affine behavior. From this interaction law, Mori–Tanaka and self-consistent schemes have been derived (Mercier and Molinari (2009)). Different and more sophisticated interaction laws were proposed based on projection operators and translated fields, again using the self-consistent approximations (Paquin et al., 1999; Sabar et al., 2002; Berbenni et al., 2004; Mareau et al., 2009). Another class of models is based on incremental variational principle, and were successively proposed for linear viscoelasticity (Lahellec and Suquet, 2007a), and nonlinear viscoelasticity (Lahellec and Suquet, 2007b,c). Recently, Doghri et al. (2010a) proposed a general incrementally affine linearization method which leads to thermo-elastic-like relations directly in the time domain. The method is very general, and can handle any elasto-viscoplastic model.

Compared to viscoelastic or elasto-(visco) plastic behavior, it appears that the homogenization of viscoelastic–viscoplastic (VE–VP) composites has received little attention up to now. Aboudi (2005) proposed a micromechanical model to predict effective properties of VE–VP composites based on the asymptotic homogenization technique. In this work the VE–VP behavior is described by the model developed by Frank and Brockman (2001) for polymer materials. Alternatively, Kim and Muliana (2010) used the method of cells and subcells to model VE–VP composites reinforced by elastic inclusions, extending a previous model in nonlinear viscoelasticity (Muliana and Kim, 2007). For the matrix phase, the nonlinear viscoelastic behavior is described by Shapery's integral model, and two viscoplastic models are considered: the Perzyna model and Valanis' endochronic theory.

In the present work, we focus our efforts on the generalization of the incrementally affine linearization method of Doghri et al. (2010a) to coupled VE–VP behavior. To this end, a general linearization procedure for viscoelastic–viscoplastic constitutive models is proposed in a time-discretized setting. The procedure leads to an incrementally affine constitutive relation in the time domain which is form-similar to a linear thermo-elastic relation. Uniform, reference properties are also defined for each phase. Then, linear mean-field homogenization models can be applied at each time step. Numerical algorithms are also provided. In order to assess the accuracy of the proposed mean-field model, reference solutions are obtained from direct FE analysis of representative cells of the microstructure.

The paper is organized as follows. The adopted constitutive equations of the coupled VE–VP response are summarized in Section 2. As the linearization technique sustaining our MFH approach makes use of algorithmic tangent operators, a computational algorithm is also presented. Section 3 presents the proposed incrementally affine linearization procedure of the constitutive equations, which constitutes the cornerstone of the MFH scheme. The linearization enables us to relate stress and strain increments by thermoelastic-like relations. The MFH procedure based on the incrementally affine linearization is then described in Section 4. Numerical predictions of the semi-analytical homogenization scheme are compared against FE simulations and experimental data in Section 5 and the results are discussed. Conclusions are drawn in Section 6.

The following acronyms are used throughout the text. VE: viscoelastic(ity), VP: viscoplastic(ity), EVP: elasto-viscoplastic (ity), VEP: Viscoelastic(ity)–plastic(ity), VE–VP: viscoelastic(ity)–viscoplastic(ity), and MFH: mean field homogenization. Boldface symbols designate second or fourth-rank tensors, as indicated by the context. Dyadic and inner products are expressed as:

$$(\boldsymbol{a}\otimes\boldsymbol{b})_{ijkl}=a_{ij}b_{kl},\quad \mathbf{a}:\mathbf{b}=a_{ij}b_{ji},\quad (\mathbf{A}:\boldsymbol{b})_{ij}=A_{ijkl}b_{lk},$$

where summation over a repeated index is supposed. The symbols $\mathbf{1}$ and $\mathbf{I}$ designate the second- and fourth-rank symmetric identity tensors, respectively. Finally, the spherical and deviatoric operators $\mathbf{I}^{vol}$ and $\mathbf{I}^{dev}$ are given by:

$$\mathbf{I}^{\mathrm{vol}}\equiv\frac{1}{3}\mathbf{1}\otimes\mathbf{1}\quad\text{and}\quad\mathbf{I}^{\mathrm{dev}}\equiv\mathbf{I}-\mathbf{I}^{\mathrm{vol}}$$

so that for $a_{ij}=a_{ji}$ we have:

$$\mathbf{I}^{\mathrm{vol}}:\mathbf{a}=\frac{1}{3}a_{mm}\mathbf{1},\quad\mathbf{I}^{\mathrm{dev}}:\mathbf{a}=\mathbf{a}-\frac{1}{3}a_{mm}\mathbf{1}\equiv\mathrm{dev}(\mathbf{a})$$

2. Homogeneous viscoelastic–viscoplastic isotropic materials

2.1. Constitutive relations

The coupled VE–VP constitutive equations considered in this work are described in detail Miled et al. (2011). They are summarized as follows. The constitutive model is based on the assumption that the total strain can be decomposed into VE and VP parts:

$$\boldsymbol{\epsilon}=\boldsymbol{\epsilon}^{\mathrm{ve}}+\boldsymbol{\epsilon}^{\mathrm{vp}}\tag{1}$$

2.1.1. Linear viscoelastic response

The Cauchy stress $\boldsymbol{\sigma}(t)$ is related to the history of VE strains $\boldsymbol{\epsilon}^{\mathrm{ve}}$ for $\tau\leqslant t$ via a linear VE model expressed by Boltzmann's hereditary integral (Boltzmann, 1878):

$$\boldsymbol{\sigma}(t)=\int_{-\infty}^{t}\mathbf{E}(t-\tau):\frac{\partial\boldsymbol{\epsilon}^{\mathrm{ve}}}{\partial\tau}d\tau\tag{2}$$

For an isotropic material, the fourth-order relaxation tensor is written as:

$$\mathbf{E}(t)=2G(t)\mathbf{I}^{\mathrm{dev}}+3K(t)\mathbf{I}^{\mathrm{vol}}\tag{3}$$

Please cite this article in press as: Miled, B., et al. Micromechanical modeling of coupled viscoelastic–viscoplastic composites based on an incrementally affine formulation. Int. J. Solids Struct. (2013), http://dx.doi.org/10.1016/j.ijsolstr.2013.02.004

where $G(t)$ and $K(t)$ are shear and bulk relaxation functions, respectively, which can be expressed in the form of Prony series:

$$G(t) = G_\infty + \sum_{i=1}^{I} G_i \exp\left(-\frac{t}{g_i}\right) \quad \text{and} \quad K(t) = K_\infty + \sum_{j=1}^{J} K_j \exp\left(-\frac{t}{k_j}\right). \tag{4}$$

Here, g_i $(i = 1 \ldots I)$ and k_j $(j = 1 \ldots J)$ are the deviatoric and volumetric relaxation times respectively; G_i $(i = 1 \ldots I)$ and K_j $(j = 1 \ldots J)$ are the corresponding moduli or weights, and G_∞ and K_∞ are the long-term elastic shear and bulk moduli.

Then, by substituting Eqs. (3) and (4) into Eq. (2), the deviatoric $(\mathbf{s}(t))$ and dilatational $(\sigma_H(t))$ parts of the stress tensor may be expressed in function of the deviatoric $(\xi(t))$ and dilatational $(\epsilon_H(t))$ parts of the strain tensor:

$$\begin{cases} \mathbf{s}(t) = 2G_\infty \boldsymbol{\xi}^{\text{ve}}(t) + \sum_{i=1}^{I} \mathbf{s}_i(t) \\ \sigma_H(t) = 3K_\infty \epsilon_H^{\text{ve}}(t) + \sum_{j=1}^{J} \sigma_{H_j}(t) \end{cases} \tag{5}$$

where viscous components are defined by:

$$\begin{cases} \mathbf{s}_i(t) \equiv 2G_i \exp\left(-\frac{t}{g_i}\right) \int_{-\infty}^{t} \exp\left(\frac{\tau}{g_i}\right) \frac{\partial \boldsymbol{\xi}^{\text{ve}}}{\partial \tau} \, d\tau \\ \sigma_{H_j}(t) \equiv 3K_j \exp\left(-\frac{t}{k_j}\right) \int_{-\infty}^{t} \exp\left(\frac{\tau}{k_j}\right) \frac{\partial \epsilon_H^{\text{ve}}}{\partial \tau} \, d\tau \end{cases} \tag{6}$$

2.1.2. Viscoplastic response

Reference Miled et al. (2011) used the classical J_2 rate-dependent model with isotropic hardening to represent the VP effects. Accordingly, the yield criterion is given as follows:

$$f(\sigma_{eq}, p, \dot{\epsilon}) \equiv \sigma_{eq} - (\sigma_y(\dot{\epsilon}) + R(p)); \quad \sigma_{eq} \equiv \sqrt{\frac{3}{2}\mathbf{s} : \mathbf{s}} \tag{7}$$

where σ_{eq} is the von Mises equivalent stress, σ_y the initial yield stress (which may depend on the strain rate) and $R(p)$ the hardening stress. The accumulated plastic strain p is an internal variable which keeps track of the past history of the VP strain:

$$p(t) = \int_0^t \dot{p}(\tau) \, d\tau \quad \text{and} \quad \dot{p} = \sqrt{\frac{2}{3}\dot{\boldsymbol{\epsilon}}^{vp} : \dot{\boldsymbol{\epsilon}}^{vp}} \tag{8}$$

The VP strain rate follows a plastic flow rule:

$$\dot{\boldsymbol{\epsilon}}^{\text{vp}} = \dot{p}\frac{\partial f}{\partial \boldsymbol{\sigma}} = \dot{p}\mathbf{N} \tag{9}$$

where the $\mathbf{N}$ tensor is given by:

$$\mathbf{N} = \frac{3}{2}\frac{\mathbf{s}}{\sigma_{eq}} \quad \text{which implies} \quad \mathbf{N} : \mathbf{N} = \frac{3}{2} \tag{10}$$

and the multiplier $\dot{p}$ is defined by a viscoplastic function g_v:

$$\begin{cases} \dot{p} = 0 & \text{if} \quad f \leqslant 0 \\ \dot{p} = g_v(\sigma_{eq}, p, \dot{\epsilon}) > 0 & \text{if} \quad f > 0 \end{cases} \tag{11}$$

2.2. Computational algorithm

The numerical algorithm proposed by Miled et al. (2011) for the coupled VE–VP behavior is based on a combination of techniques which were previously used separately for VE and EVP models (e.g., Simo and Hughes, 1998). Two approaches have been considered to compute the integrals of Eq. (6) over $t \in [t_n, t_{n+1}]$. The first one supposes that the VE strain rate is constant over the time interval, and the second method is the mid-point integration rule. The two methods lead to the definition of incremental relaxation moduli $\widetilde{G}(\Delta t)$ and $\widetilde{K}(\Delta t)$ which are functions of the time increment Δt (the symbol Δ designates an increment over the given time interval). The remaining blocks of the computational algorithm are written in a unified manner for both integration methods using $\widetilde{G}(\Delta t)$ and $\widetilde{K}(\Delta t)$:

$$\begin{cases} \mathbf{s}(t_{n+1}) = 2G_\infty \boldsymbol{\xi}^{\text{ve}}(t_n) + 2\widetilde{G}\Delta\boldsymbol{\xi}^{\text{ve}} + \sum_{i=1}^{I} \exp\left(-\frac{\Delta t}{g_i}\right) \mathbf{s}_i(t_n) \\ \sigma_H(t_{n+1}) = 3K_\infty \epsilon_H^{\text{ve}}(t_n) + 3\widetilde{K}\Delta\epsilon_H^{\text{ve}} + \sum_{j=1}^{J} \exp\left(-\frac{\Delta t}{k_j}\right) \sigma_{H_j}(t_n) \end{cases} \tag{12}$$

where $\widetilde{G}$ and $\widetilde{K}$ are defined for the first method as follows:

$$\begin{cases} \widetilde{G} \equiv G_\infty + \sum_{i=1}^{I} G_i \left[1 - \exp\left(-\frac{\Delta t}{g_i}\right)\right] \frac{g_i}{\Delta t} \\ \widetilde{K} \equiv K_\infty + \sum_{j=1}^{J} K_j \left[1 - \exp\left(-\frac{\Delta t}{k_j}\right)\right] \frac{k_j}{\Delta t}. \end{cases} \tag{13}$$

and for the second method:

$$\widetilde{G} = G\left(\frac{\Delta t}{2}\right) \quad \text{and} \quad \widetilde{K} = K\left(\frac{\Delta t}{2}\right) \tag{14}$$

A return mapping algorithm has been proposed based on two-steps, VE predictor followed by VP corrector. The unknown stress at t_{n+1} is expressed in a remarkably simple manner:

$$\boldsymbol{\sigma}(t_{n+1}) = \boldsymbol{\sigma}^{\text{pred}}(t_{n+1}) - \widetilde{\mathbf{E}} : \Delta\boldsymbol{\epsilon}^{\text{vp}} \tag{15}$$

with:

$$\boldsymbol{\sigma}^{\text{pred}}(t_{n+1}) = \mathbf{E}_\infty : \boldsymbol{\epsilon}^{\text{ve}}(t_n) + \widetilde{\mathbf{E}} : \Delta\boldsymbol{\epsilon} + \sum_{i=1}^{I} \exp\left(-\frac{\Delta t}{g_i}\right) \mathbf{s}_i(t_n) + \sum_{j=1}^{J} \exp\left(-\frac{\Delta t}{k_j}\right) \sigma_{H_j}(t_n)\mathbf{1} \tag{16}$$

where $\mathbf{E}_\infty = 2G_\infty \mathbf{I}^{\text{dev}} + 3K_\infty \mathbf{I}^{\text{vol}}$ and $\widetilde{\mathbf{E}} = 2\widetilde{G}\mathbf{I}^{\text{dev}} + 3\widetilde{K}\mathbf{I}^{\text{vol}}$. The total stress tensor can be written at t_n using Eq. (5):

$$\boldsymbol{\sigma}(t_n) = \mathbf{E}_\infty : \boldsymbol{\epsilon}^{\text{ve}}(t_n) + \sum_{i=1}^{I} \mathbf{s}_i(t_n) + \sum_{j=1}^{J} \sigma_{H_j}(t_n)\mathbf{1} \tag{17}$$

Combining Eqs. (15) and (17), we find the following expression of the stress increment $(\Delta\boldsymbol{\sigma} = \boldsymbol{\sigma}(t_{n+1}) - \boldsymbol{\sigma}(t_n))$:

$$\Delta\boldsymbol{\sigma} = \widetilde{\mathbf{E}} : (\Delta\boldsymbol{\epsilon} - \Delta\boldsymbol{\epsilon}^{\text{vp}}) + \mathbf{a}(t_n) \tag{18}$$

where $\mathbf{a}(t_n)$ is the following second-order tensor:

$$\mathbf{a}(t_n) = -\sum_i \left[1 - \exp\left(-\frac{\Delta t}{g_i}\right)\right] \mathbf{s}_i(t_n) - \sum_j \left[1 - \exp\left(-\frac{\Delta t}{k_j}\right)\right] \sigma_{H_j}(t_n)\mathbf{1} \tag{19}$$

The stress–strain incremental relation Eq. (18) is very similar to the EVP case except that we use a viscoelastic tangent operator $\widetilde{\mathbf{E}}$ (which is a function of Δt) instead of a (constant) elastic stiffness operator and we have introduced a second-order tensor $\mathbf{a}(t_n)$ (which is nil in EVP). Contrary to elasto-plasticity, there is no one-to-one correspondence between stress and strain rates in a VE–VP model. However, when considering finite strain and stress increments instead of infinitesimal ones, an algorithmic tangent operator $\mathbf{C}^{\text{alg}}$ may be derived from a consistent linearization of the time-discretized constitutive equations around the solution at t_{n+1}:

$$\delta\boldsymbol{\sigma}(t_{n+1}) = \mathbf{C}^{\text{alg}} : \delta\boldsymbol{\epsilon}(t_{n+1}) \tag{20}$$

where δ designates a total variation at t_{n+1} (thus $\delta\mathbf{x}(t_n) = 0$, where $\mathbf{x}$ designates a variable).Radial return mapping described above for

Please cite this article in press as: Miled, B., et al. Micromechanical modeling of coupled viscoelastic–viscoplastic composites based on an incrementally affine formulation. Int. J. Solids Struct. (2013), http://dx.doi.org/10.1016/j.ijsolstr.2013.02.004

the VE–VP model is similar to the classical EVP case. Hence, the algorithmic tangent operator is derived by adopting a similar reasoning as for J_2 EVP. After some mathematical developments (see Miled et al., 2011), the following *remarkably simple* expression is obtained:

$$\mathbf{C}^{\text{alg}} = \widetilde{\mathbf{E}} - \frac{\left(2\widetilde{G}\right)^2}{h_v}\mathbf{N}\otimes\mathbf{N} - \left(2\widetilde{G}\right)^2 \frac{\sigma_{eq}\Delta p}{\sigma_{eq}+3\widetilde{G}\Delta p}\frac{\partial \mathbf{N}}{\partial \boldsymbol{\sigma}} - \frac{2\widetilde{G}}{h_v g_{,\sigma}}\mathbf{N}\otimes g_{,\epsilon} \tag{21}$$

where the rate-dependent denominator h_v is defined by this expression:

$$h_v \equiv \frac{1}{(\Delta t)g_{,\sigma}} + 3\widetilde{G} - \frac{g_{,p}}{g_{,\sigma}} \tag{22}$$

$$\text{Notations}: g_{,\sigma} \equiv \frac{\partial g_v}{\partial \sigma_{eq}}; \quad g_{,p} \equiv \frac{\partial g_v}{\partial p}; \quad g_{,\epsilon} \equiv \frac{1}{\Delta t}\frac{\partial g_v}{\partial \dot{\epsilon}}$$

When the initial yield stress σ_y is constant then $g_{,\epsilon} = \mathbf{0}$, and the algorithmic tangent operator becomes symmetric and *form-identical* to its expression in EVP in Doghri (2000, e.g. chapter 13) provided that the incremental relaxation moduli $\widetilde{G}$ and $\widetilde{K}$ replace the constant elastic moduli G and K.

The expressions of $g_{,\sigma}$ and $g_{,p}$ depend on the considered VP function. For example, using Norton's power law:

$$g_v(\sigma_{eq}, p) = \begin{cases} \frac{\sigma_y}{\eta}\left(\frac{f}{\sigma_y}\right)^m & \text{if} \quad f > 0 \\ 0, & \text{otherwise} \end{cases} \tag{23}$$

where η[Pa s] and m are the viscoplastic modulus and exponent, respectively. We can easily compute:

$$g_{,\sigma} = \frac{m}{\eta}\left(\frac{f}{\sigma_y}\right)^{m-1}, \quad \frac{g_{,p}}{g_{,\sigma}} = -\frac{dR}{dp}, \quad h_v = \frac{\eta}{m(\Delta t)}\left(\frac{f}{\sigma_y}\right)^{1-m} + 3\widetilde{G} + \frac{dR}{dp}$$

The overstress can also be considered using another power-law VP function with two parameters: the viscoplastic modulus (κ[1/s]) and exponent (m) which appear as follows:

$$g_v(\sigma_{eq}, p) = \begin{cases} \kappa\left(\frac{f}{\sigma_y + R(p)}\right)^m & \text{if} \quad f > 0 \\ 0, & \text{otherwise} \end{cases} \tag{24}$$

For this case:

$$g_{,\sigma} = m\frac{g_v}{f}, \quad g_{,p} = -m g_v \frac{dR}{dp}\left(\frac{1}{f} + \frac{1}{\sigma_y + R(p)}\right),$$
$$h_v = \frac{f}{m g_v(\Delta t)} + 3\widetilde{G} + \frac{dR}{dp}\frac{\sigma_{eq}}{\sigma_y + R(p)}$$

From the algorithmic tangent operator computed for the coupled VE–VP case, we may retrieve the operator for traditional types of constitutive equations:

1. *From VE–VP to linear viscoelasticity*: This case is obtained when the initial yield stress (σ_y) tends to $+\infty$. The VE predictor is always the solution, and terms in Eq. (21) which are due to the evolution of VP strains (i.e. $\mathbf{N}$ and $\frac{\partial \mathbf{N}}{\partial \boldsymbol{\sigma}}$ terms) vanish. This gives:

$$\mathbf{C}^{\text{alg}} = \widetilde{\mathbf{E}} \tag{25}$$

2. *From VE–VP to elasto-viscoplasticity*: This case is obtained when the shear and bulk relaxation times tend to $+\infty$, and when the initial yield stress is constant.

$$\mathbf{C}^{\text{alg}} = \mathbf{E}^{\text{el}} - \frac{(2G)^2}{h_v}\mathbf{N}\otimes\mathbf{N} - (2G)^2\frac{\sigma_{eq}\Delta p}{\sigma_{eq}+3G\Delta p}\frac{\partial \mathbf{N}}{\partial \boldsymbol{\sigma}} \tag{26}$$

where:

$$\mathbf{E}^{\text{el}} = 2G\mathbf{I}^{\text{dev}} + 3K\mathbf{I}^{\text{vol}}, \quad G = G_\infty + \sum_{i=1}^{I} G_i, \quad K = K_\infty + \sum_{j=1}^{J} K_j$$

$$h_v \equiv \frac{1}{(\Delta t)g_{,\sigma}} + 3G - \frac{g_{,p}}{g_{,\sigma}}$$

2.3. Regularization of the algorithmic tangent operator

Starting from Eq. (22), it can be shown that $h_v \to \infty$ for very small time increments ($\Delta t \to 0$), which is unacceptable (because then $\mathbf{C}^{\text{alg}}$ approaches $\widetilde{\mathbf{E}}$ although $\boldsymbol{\epsilon}^{\text{vp}} \neq \mathbf{0}$). In order to solve the problem, Doghri et al. (2010a) developed a regularization method in EVP starting from a 1D analytical tangent expression valid for the most simple case (monotonic uniaxial tension, constant strain rate, linear isotropic hardening and linear viscous stress).

A similar development leading to a regularized tangent operator for coupled VE–VP behavior starting from the 1D analytical solution proposed by Miled et al. (2011) is a difficult task even for the most simple case. Instead, in the present work we propose a direct generalization of $\mathbf{C}^{\text{reg}}$ from EVP to VE–VP case:

$$\mathbf{C}^{\text{reg}}(t_{n+1}) = \mathbf{C}^{\text{vep}}(t_{n+1}) + \left(\mathbf{C}^{\text{reg}}(t_n) - \mathbf{C}^{\text{vep}}(t_{n+1})\right)\exp\left(-\frac{h_{\text{vep}}}{h_v - h_{\text{vep}}}\right) \tag{27}$$

where $\mathbf{C}^{\text{vep}}(t_{n+1})$ and h_{vep} are expressed as follows:

$$\mathbf{C}^{\text{vep}} = \widetilde{\mathbf{E}} - \frac{\left(2\widetilde{G}\right)^2}{h_{\text{vep}}}\mathbf{N}\otimes\mathbf{N}, \quad h_{\text{vep}} = 3\widetilde{G} - \frac{g_{,p}}{g_{,\sigma}} \tag{28}$$

From Eq. (27), we can show that when $\Delta t \to 0$, then $\mathbf{C}^{\text{reg}}(t_{n+1})$ tends to $\mathbf{C}^{\text{reg}}(t_n)$ (because $\exp\left(-\frac{h_{\text{vep}}}{h_v - h_{\text{vep}}}\right) = \exp\left(-\Delta t g_{,\sigma}(3\widetilde{G} - \frac{g_{,p}}{g_{,\sigma}})\right) \underbrace{\to}_{\Delta t \to 0} 1$; $g_{,\sigma}$ and $\frac{g_{,p}}{g_{,\sigma}}$ are independent of Δt, and $\widetilde{G} \underbrace{\to}_{\Delta t \to 0} G$), and not to the VE tangent operator $\widetilde{\mathbf{E}}$, as in the case of the algorithmic tangent operator. From the same equation, the expression of the regularized tangent operator for the EVP behavior is recovered when the shear and bulk relaxation times tend to $+\infty$.

For rate-dependent VE–VP, $\mathbf{C}^{\text{reg}}(t_{n+1})$ is the regularized tangent operator that is used later in mean-field homogenization, instead of the original algorithmic tangent $\mathbf{C}^{\text{alg}}(t_{n+1})$ of Eq. (21). Numerical experience showed that $\mathbf{C}^{\text{reg}}(t_{n+1})$ is quite insensitive to the value of Δt and behaves correctly for vanishingly small Δt.

3. Incrementally affine linearization method

The main purpose of this section is to relate the increments of stress and strain via a tangent operator. This is needed later for the homogenization of VE–VP composites.

3.1. General presentation

Consider the same general viscoplastic model studied by Doghri et al. (2010a). The evolution equations of the VP strain $\boldsymbol{\epsilon}^{\text{vp}}$ and the scalar and/or tensor internal variables $\mathbf{V}$ are given by these expressions:

$$\dot{\boldsymbol{\epsilon}}^{\text{vp}}(t) = \tilde{\boldsymbol{\epsilon}}(\boldsymbol{\sigma}(t), \quad \mathbf{V}(t)), \dot{\mathbf{V}}(t) = \tilde{\mathbf{V}}(\boldsymbol{\sigma}(t), \mathbf{V}(t)) \tag{29}$$

$$\text{Notations}: \tilde{\boldsymbol{\epsilon}}_{,\boldsymbol{\sigma}} \equiv \frac{\partial \tilde{\boldsymbol{\epsilon}}}{\partial \boldsymbol{\sigma}}; \quad \tilde{\boldsymbol{\epsilon}}_{,\mathbf{V}} \equiv \frac{\partial \tilde{\boldsymbol{\epsilon}}}{\partial \mathbf{V}}; \quad \tilde{\mathbf{V}}_{,\boldsymbol{\sigma}} \equiv \frac{\partial \tilde{\mathbf{V}}}{\partial \boldsymbol{\sigma}}; \quad \tilde{\mathbf{V}}_{,\mathbf{V}} \equiv \frac{\partial \tilde{\mathbf{V}}}{\partial \mathbf{V}}$$

Please cite this article in press as: Miled, B., et al. Micromechanical modeling of coupled viscoelastic–viscoplastic composites based on an incrementally affine formulation. Int. J. Solids Struct. (2013), http://dx.doi.org/10.1016/j.ijsolstr.2013.02.004

The previous equations are linearized at time t close to a time τ:

$$\dot{\boldsymbol{\epsilon}}^{\mathrm{vp}}(t) = \dot{\boldsymbol{\epsilon}}^{\mathrm{vp}}(\tau) + \tilde{\boldsymbol{\epsilon}}_{,\boldsymbol{\sigma}}(\tau) : (\boldsymbol{\sigma}(t) - \boldsymbol{\sigma}(\tau)) + \tilde{\boldsymbol{\epsilon}}_{,\mathbf{V}}(\tau) \bullet (\mathbf{V}(t) - \mathbf{V}(\tau)) \tag{30}$$

$$\dot{\mathbf{V}}(t) = \dot{\mathbf{V}}(\tau) + \tilde{\mathbf{V}}_{,\boldsymbol{\sigma}}(\tau) : (\boldsymbol{\sigma}(t) - \boldsymbol{\sigma}(\tau)) + \tilde{\mathbf{V}}_{,\mathbf{V}}(\tau) \bullet (\mathbf{V}(t) - \mathbf{V}(\tau)) \tag{31}$$

The bullet symbol "$\bullet$" designates a sum of inner products, e.g., if $\mathbf{V} = (p, \mathbf{X})$, then:

$$\tilde{\boldsymbol{\epsilon}}_{,\mathbf{V}} \bullet \delta\mathbf{V} = \tilde{\boldsymbol{\epsilon}}_{,p}\delta p + \tilde{\boldsymbol{\epsilon}}_{,\mathbf{X}} : \delta\mathbf{X}$$

The linearized evolution equations (Eqs. (30) and (31)) are then discretized using a fully implicit backward Euler time integration algorithm while choosing $(t = t_n, \tau = t_{n+1})$. The resulting time discrete form of these equations is:

$$\begin{cases} \frac{1}{\Delta t}\Delta\boldsymbol{\epsilon}^{\mathrm{vp}} = \dot{\boldsymbol{\epsilon}}^{\mathrm{vp}}(t_n) + \tilde{\boldsymbol{\epsilon}}_{,\boldsymbol{\sigma}}(t_{n+1}) : \Delta\boldsymbol{\sigma} + \tilde{\boldsymbol{\epsilon}}_{,\mathbf{V}}(t_{n+1}) \bullet \Delta\mathbf{V} \\ \frac{1}{\Delta t}\Delta\mathbf{V} = \dot{\mathbf{V}}(t_n) + \tilde{\mathbf{V}}_{,\boldsymbol{\sigma}}(t_{n+1}) : \Delta\boldsymbol{\sigma} + \tilde{\mathbf{V}}_{,\mathbf{V}}(t_{n+1}) \bullet \Delta\mathbf{V} \end{cases} \tag{32}$$

We can rewrite the second equation of system (32) as follows:

$$\left[\frac{1}{\Delta t}\mathbf{I} - \tilde{\mathbf{V}}_{,\mathbf{V}}(t_{n+1})\right] \bullet \Delta\mathbf{V} = \dot{\mathbf{V}}(t_n) + \tilde{\mathbf{V}}_{,\boldsymbol{\sigma}}(t_{n+1}) : \Delta\boldsymbol{\sigma} \tag{33}$$

Combination of the first equation of system (32) with Eq. (33) gives:

$$\Delta\boldsymbol{\epsilon}^{\mathrm{vp}} = \left[\dot{\boldsymbol{\epsilon}}^{\mathrm{vp}}(t_n) + \tilde{\boldsymbol{\epsilon}}_{,\mathbf{V}}(t_{n+1}) \bullet [\ldots]^{-1} \bullet \dot{\mathbf{V}}(t_n) + \{\ldots\} : \Delta\boldsymbol{\sigma}\right]\Delta t \tag{34}$$

where the expressions of $[\ldots]$ and $\{\ldots\}$ are given by:

$$[\ldots] = \frac{1}{\Delta t}\mathbf{I} - \tilde{\mathbf{V}}_{,\mathbf{V}}(t_{n+1}) \tag{35}$$

$$\{\ldots\} = \tilde{\boldsymbol{\epsilon}}_{,\boldsymbol{\sigma}}(t_{n+1}) + \tilde{\boldsymbol{\epsilon}}_{,\mathbf{V}}(t_{n+1}) \bullet [\ldots]^{-1} \bullet \tilde{\mathbf{V}}_{,\boldsymbol{\sigma}}(t_{n+1}) \tag{36}$$

We note that Eq. (29) → Eq. (36) are the same as those of EVP case (see Doghri et al., 2010a). After substituting the expression of $\Delta\boldsymbol{\epsilon}^{\mathrm{vp}}$ (Eq. (34)) in Eq. (18), the following final result is reached:

$$\boxed{\Delta\boldsymbol{\sigma} = \mathbf{C}^{\mathrm{alg}}(t_{n+1}) : (\Delta\boldsymbol{\epsilon} - \Delta\boldsymbol{\epsilon}^{\mathrm{af}})} \tag{37}$$

where the algorithmic tangent operator at time t_{n+1} ($\mathbf{C}^{\mathrm{alg}}(t_{n+1})$) and the affine strain increment ($\Delta\boldsymbol{\epsilon}^{\mathrm{af}}$) are expressed as follows (see A):

$$\mathbf{C}^{\mathrm{alg}}(t_{n+1}) = \left(\widetilde{\mathbf{E}}^{-1} + \Delta t\{\ldots\}\right)^{-1}$$

$$\Delta\boldsymbol{\epsilon}^{\mathrm{af}} \equiv \Delta\boldsymbol{\epsilon}^{\mathrm{af}}_{\mathrm{evp}} - \widetilde{\mathbf{E}}^{-1} : \mathbf{a}(t_n) \tag{38}$$

where $\Delta\boldsymbol{\epsilon}^{\mathrm{af}}_{\mathrm{evp}}$ is given by this expression:

$$\Delta\boldsymbol{\epsilon}^{\mathrm{af}}_{\mathrm{evp}} \equiv \left[\dot{\boldsymbol{\epsilon}}^{\mathrm{vp}}(t_n) + \tilde{\boldsymbol{\epsilon}}_{,\mathbf{V}}(t_{n+1}) \bullet [\ldots]^{-1} \bullet \dot{\mathbf{V}}(t_n)\right]\Delta t \tag{39}$$

Replacing the expressions of $\widetilde{\mathbf{E}}^{-1}$ and $\mathbf{a}(t_n)$ in the general equation of $\Delta\boldsymbol{\epsilon}^{\mathrm{af}}$ (Eq. (38)), we find:

$$\Delta\boldsymbol{\epsilon}^{\mathrm{af}} = \Delta\boldsymbol{\epsilon}^{\mathrm{af}}_{\mathrm{evp}} + \frac{1}{2\widetilde{G}}\sum_i \left[1 - \exp\left(-\frac{\Delta t}{g_i}\right)\right]\mathbf{s}_i(t_n) + \frac{1}{3\widetilde{K}}\sum_j \left[1 - \exp\left(-\frac{\Delta t}{k_j}\right)\right]\sigma_{H_j}(t_n)\mathbf{1} \tag{40}$$

To recover the EVP results from the incrementally affine relation Eq. (37), it suffices to choose $g_i \to +\infty$ and $k_j \to +\infty$. In this case, the second-order tensor $\mathbf{a}(t_n)$ expressed by Eq. (19) vanishes, and, hence: $\Delta\boldsymbol{\epsilon}^{\mathrm{af}} = \Delta\boldsymbol{\epsilon}^{\mathrm{af}}_{\mathrm{evp}}$, which is the EVP affine strain increment given in Doghri et al. (2010a).Contrary to the original formulation (Masson and Zaoui, 1999; Pierard and Doghri, 2006a), the incrementally affine formulation Eq. (37) is directly affine in the time domain, and not in the Laplace–Carson one. In addition, it is very general, and it is valid for any viscoplastic model described by a set of scalar and/or tensor variables $\mathbf{V}$. Finally, it is very similar to that of EVP case except that we use a viscoelasic tangent operator instead of an elastic stiffness and we have a second-order tensor $\mathbf{a}(t_n) \neq \mathbf{0}$ instead of a null tensor.

3.2. Application to J_2 constitutive model

In J_2 viscoplasticity, the evolution equations of the VP strain $\boldsymbol{\epsilon}^{\mathrm{vp}}$ and the scalar internal variable $V = p$ are given by these expressions:

$$\dot{\boldsymbol{\epsilon}}^{\mathrm{vp}}(t) = \tilde{\boldsymbol{\epsilon}}(\boldsymbol{\sigma}(t), p(t)) = g_v(\sigma_{eq}, p)\mathbf{N} \tag{41}$$

$$\dot{p}(t) = \tilde{p}(\boldsymbol{\sigma}(t), p(t)) = g_v(\sigma_{eq}, p) \tag{42}$$

The partial derivatives of the previous functions give:

$$\tilde{p}_{,\boldsymbol{\sigma}} = \frac{\partial g_v}{\partial \sigma_{eq}}\mathbf{N}, \quad \tilde{p}_{,p} = \frac{\partial g_v}{\partial p} \tag{43}$$

$$\tilde{\boldsymbol{\epsilon}}_{,\boldsymbol{\sigma}} = \tilde{p}\frac{\partial \mathbf{N}}{\partial \boldsymbol{\sigma}} + \mathbf{N} \otimes \tilde{p}_{,\boldsymbol{\sigma}}, \quad \tilde{\boldsymbol{\epsilon}}_{,p} = \tilde{p}_{,p}\mathbf{N} \tag{44}$$

Replacing the expressions of the partial derivatives (Eqs. (43) and (44)) in the general equation of the affine strain increment for the EVP behavior $\Delta\boldsymbol{\epsilon}^{\mathrm{af}}_{\mathrm{evp}}$ (Eq. (39)), we find:

$$\Delta\boldsymbol{\epsilon}^{\mathrm{af}}_{\mathrm{evp}} = \dot{p}(t_n)\Delta t\left[\mathbf{N}(t_n) + \mathbf{N}(t_{n+1})\frac{g_{,p}(t_{n+1})\Delta t}{1 - g_{,p}(t_{n+1})\Delta t}\right] \tag{45}$$

The last relation is a function of $\Delta t, \dot{p}(t_n), \mathbf{N}(t_n), \mathbf{N}(t_{n+1})$ and $g_{,p}(t_{n+1})$. The linearization method can be extended to more sophisticated models combining both nonlinear isotropic and kinematic hardenings. This extension is already available for the elasto-viscoplastic case (Doghri et al., 2010a).

4. Mean-field homogenization (MFH) of VE–VP composites

4.1. Analogy with thermoelasticity

We now address the homogenization of two-phase composites having VE–VP phases. In the sequel, subscripts 0 and 1 designate matrix and inclusion phases, respectively, and $\langle\rangle_{w_0}, \langle\rangle_{w_1}$ and $\langle\rangle$ designate volume averages over matrix, inclusions and representative volume element (RVE) domains, respectively.

We have shown in the last section that a VE–VP response can be expressed in the incrementally affine form (Eq. (37)). Actually, this equation is form-similar to linear thermoelasticity, so that available homogenization models for linear thermoelastic composites can be applied at each time step. Indeed, for a linear thermoelastic composite, the local constitutive response can be written as:

$$\begin{aligned} \boldsymbol{\sigma}(x) &= \mathbf{E}^{\mathrm{el}}(x) : (\boldsymbol{\epsilon}(x) - \boldsymbol{\epsilon}^{\mathrm{th}}(x)), \quad \boldsymbol{\epsilon}^{\mathrm{th}}(x) = \boldsymbol{\alpha}(x)\Delta T \\ &= \mathbf{E}^{\mathrm{el}}(x) : \boldsymbol{\epsilon}(x) + \boldsymbol{\beta}(x), \quad \boldsymbol{\beta}(x) = -\mathbf{E}^{\mathrm{el}}(x) : \boldsymbol{\alpha}(x)\Delta T \end{aligned} \tag{46}$$

where $\mathbf{E}^{\mathrm{el}}(x)$ is the elastic stiffness, $\boldsymbol{\alpha}(x)$ the thermal expansion, and ΔT is a change in temperature. Based on Eq. (37), application of thermoelastic models to the present VE–VP composites can be achieved provided that for each time interval the following substitutions are made:

$$\boldsymbol{\sigma} \to \Delta\boldsymbol{\sigma}, \quad \mathbf{E}^{\mathrm{el}} \to \mathbf{C}^{\mathrm{tan}}, \quad \boldsymbol{\epsilon} \to \Delta\boldsymbol{\epsilon}, \quad (\boldsymbol{\beta}) \to -\mathbf{C}^{\mathrm{tan}} : \Delta\boldsymbol{\epsilon}^{\mathrm{af}} \tag{47}$$

where $\mathbf{C}^{\mathrm{tan}}$ designates a tangent operator. The incrementally affine relation (37) is rigorously valid for the algorithmic tangent, $\mathbf{C}^{\mathrm{tan}} = \mathbf{C}^{\mathrm{alg}}$. However, and as discussed in Section 2.3, for MFH we use the regularized tangent operator of Eq. (27), i.e. $\mathbf{C}^{\mathrm{tan}} = \mathbf{C}^{\mathrm{reg}}$. Classical relations for the effective properties of linear thermo-elastic composites are given in B. However, when VP strains evolve within a phase,the tangent operator is not homogeneous within the phase, preventing the direct application of the linear schemes described

Please cite this article in press as: Miled, B., et al. Micromechanical modeling of coupled viscoelastic–viscoplastic composites based on an incrementally affine formulation. Int. J. Solids Struct. (2013), http://dx.doi.org/10.1016/j.ijsolstr.2013.02.004

here-above. A similar problem affects the affine strain increment per phase (whether VP strains evolve or not). A workaround is to define uniform, reference comparison operators $\hat{\mathbf{C}}_r^{\tan}(t)$ and $\Delta\hat{\boldsymbol{\epsilon}}_r^{\mathrm{af}}(t)$ for each phase (r), computed in this work from the constitutive equations of the phases evaluated at the phase average of the strain in the phase. Using the substitutions of Eq. (47), the macroscopic thermo-elastic expression (Eq. (B.3) in Appendix B) is then rewritten as follows:

$$\langle\Delta\boldsymbol{\sigma}\rangle = \bar{\mathbf{C}} : \langle\Delta\boldsymbol{\epsilon}\rangle - v_0\hat{\mathbf{C}}_0^{\tan} : \Delta\hat{\boldsymbol{\epsilon}}_0^{\mathrm{af}} - v_1\hat{\mathbf{C}}_1^{\tan} : \Delta\hat{\boldsymbol{\epsilon}}_1^{\mathrm{af}} - v_1(\hat{\mathbf{C}}_1^{\tan} - \hat{\mathbf{C}}_0^{\tan}) : (\mathbf{A} - \mathbf{I}) : (\hat{\mathbf{C}}_1^{\tan} - \hat{\mathbf{C}}_0^{\tan})^{-1} : (\hat{\mathbf{C}}_1^{\tan} : \Delta\hat{\boldsymbol{\epsilon}}_1^{\mathrm{af}} - \hat{\mathbf{C}}_0^{\tan} : \Delta\hat{\boldsymbol{\epsilon}}_0^{\mathrm{af}}) \tag{48}$$

The comparison tangent operators for the matrix ($\hat{\mathbf{C}}_0^{\tan}$) and inclusion ($\hat{\mathbf{C}}_1^{\tan}$) phases are uniform and anisotropic, by construction.

4.2. Isotropisation of the tangent operator

Predictions of the incremental or affine formulations are known to be too stiff and this is illustrated for instance by Pierard (2006); Pierard and Doghri, 2006b for elasto-plastic or elasto-viscoplastic composites. Various attempts to soften the response are presented in the literature. The key idea is to consider tensors other than anisotropic tangent tensors ($\mathbf{C}^{\mathrm{ani}}$) in the computation of the Eshelby, Hill and effective tangent tensors. This can be done by extracting an isotropic part of the given anisotropic tensors. To do this, we must find two scalars μ_t and k_t from $\mathbf{C}^{\mathrm{ani}}$ so that the fourth-order isotropic projection ($\mathbf{C}^{\mathrm{iso}}$) is written as follows:

$$\mathbf{C}^{\mathrm{iso}} = 2\mu_t\mathbf{I}^{\mathrm{dev}} + 3k_t\mathbf{I}^{\mathrm{vol}} \tag{49}$$

The "tangent" shear (μ_t) and bulk (k_t) moduli depend on the chosen extraction method. We present hereafter a so-called special isotropisation method. The inspiration for the method comes from a spectral decomposition of certain expressions of $\mathbf{C}^{\mathrm{ani}}$ proposed by Castañeda (1996). His decomposition applies to $\mathbf{C}^{\mathrm{ani}}$ which can be cast as follows:

$$\mathbf{C}^{\mathrm{ani}} = 3k_1\mathbf{I}^{\mathrm{vol}} + 2k_2\left(\mathbf{I}^{\mathrm{dev}} - \frac{2}{3}\mathbf{N}\otimes\mathbf{N}\right) + 2k_3\left(\frac{2}{3}\mathbf{N}\otimes\mathbf{N}\right) \tag{50}$$

with $N_{ii} = 0$ and $\mathbf{N} : \mathbf{N} = \frac{3}{2}$. The spectral isotropisation method as presented in Castañeda (1996) or Pierard and Doghri (2006b) *cannot* be applied directly to the VE–VP case. However, we took inspiration from the existing method to propose in C a special isotropisation for the incrementally affine formulation of Eq. (37) by introducing four hypotheses:

1. $\mathbf{N}_{n+1} = \mathbf{N}_n$ ($\Rightarrow \Delta\boldsymbol{\epsilon}_{\mathrm{evp}}^{\mathrm{af}}$ // $\mathbf{N}$), where "//" means 'is collinear with'.
2. dev ($\Delta\boldsymbol{\epsilon}$) // $\mathbf{N}$, (true for $\Delta\boldsymbol{\epsilon}^{\mathrm{vp}}$, and a hypothesis for dev ($\Delta\boldsymbol{\epsilon}^{\mathrm{ve}}$))
3. dev ($\Delta\boldsymbol{\epsilon}^{\mathrm{af}}$) // $\mathbf{N}$ (true for $\Delta\boldsymbol{\epsilon}_{\mathrm{evp}}^{\mathrm{af}}$ if $\mathbf{N}_{n+1} = \mathbf{N}_n$, and a hypothesis for dev ($\tilde{\mathbf{E}}^{-1} : \mathbf{a}(t_n)$))
4. The initial yield stress σ_y is constant ($\Rightarrow g_{,\epsilon} = \mathbf{0}$).

According to the first three assumptions, the loading is proportional during a given time step. This was also assumed in the original spectral isotropisation method which was proposed for elasto-plasticity. Nevertheless, the resulting isotropic tangent operator will be used for all kinds of loading histories, including non-monotonic ones.

The tangent bulk and shear moduli k_t and μ_t are then found as follows:

$$k_t = k_1, \mu_t = k_3 \tag{51}$$

An application to algorithmic tangent operator of J_2 viscoplasticity gives (see Appendix C):

$$k_t = \widetilde{K}, \quad \mu_t = \widetilde{G}\left(1 - \frac{3\widetilde{G}}{h_v}\right) \tag{52}$$

which is form-identical to EVP (Doghri et al., 2010a) except that the incremental relaxation shear modulus $\widetilde{G}$ replaces the constant elastic shear modulus.

As explained in Section 2.3, the regularized tangent operator has been used in this work, instead of the original algorithmic tangent, for all numerical simulations in order to obtain good predictions for small time increments. In particular, reference, regularized tangent operators $\mathbf{C}^{\mathrm{reg}}$ are used at every occurrence of $\hat{\mathbf{C}}_r^{\tan}$ ($r = 0, 1$) in Eq. (48). The tangent shear modulus associated with the isotropisation of the regularized tangent $\mathbf{C}^{\mathrm{reg}}(t_{n+1})$ of Eq. (27) is computed as follows:

$$\mu^{\mathrm{reg}}(t_{n+1}) = \mu^{\mathrm{vep}}(t_{n+1}) + (\mu^{\mathrm{reg}}(t_n) - \mu^{\mathrm{vep}}(t_{n+1}))\exp\left(-\frac{h_{\mathrm{vep}}}{h_v - h_{\mathrm{vep}}}\right) \tag{53}$$

where $\mu^{\mathrm{vep}}(t_{n+1})$ is the tangent shear modulus obtained from the special isotropisation of $\mathbf{C}^{\mathrm{vep}}(t_{n+1})$ (Eq. (28)):

$$\mu^{\mathrm{vep}}(t_{n+1}) = \widetilde{G}\left(1 - \frac{3\widetilde{G}}{h_{\mathrm{vep}}}\right) \tag{54}$$

Let us remark that even if $\mu^{\mathrm{vep}}(t_{n+1})$ and $\mu^{\mathrm{reg}}(t_n)$ were computed from the special isotropisation of $\mathbf{C}^{\mathrm{vep}}(t_{n+1})$ and $\mathbf{C}^{\mathrm{reg}}(t_n)$, respectively, $\mu^{\mathrm{reg}}(t_{n+1})$ computed from (53) does not necessarily correspond to the special isotropisation of $\mathbf{C}^{\mathrm{reg}}(t_{n+1})$. Indeed, $\mathbf{C}^{\mathrm{reg}}(t_{n+1})$ cannot be cast in general under the form (50) needed by the special isotropisation method. In summary, $\mu^{\mathrm{vep}}(t_{n+1})$ is computed by special isotropisation while $\mu^{\mathrm{reg}}(t_{n+1})$ is given by the recurrence formula (53).

The expressions of h_{vep} for two different VP functions are given as follows:

$$h_{\mathrm{vep}} = \begin{cases} 3\widetilde{G} + \frac{dR}{dp}, & \text{Norton's power law — Eq. (23) —} \\ 3\widetilde{G} + \frac{dR}{dp}\frac{\sigma_{eq}}{\sigma_y + R(p)}, & \text{another power law approach — Eq. (24) —} \end{cases} \tag{55}$$

In order to recover the EVP case, it suffices to choose $g_i \to +\infty$ and $k_j \to +\infty$. In this case $\widetilde{G}$ and h_{vep} are remplaced by G (see Eq. (26)) and h_{ep} $\left(= 3G + \frac{dR}{dp}\right)$, respectively.

4.3. Numerical implementation

In order to compute the macro stress $\bar{\boldsymbol{\sigma}}_{n+1}$ and the macroscopic tangent operator $\bar{\mathbf{C}}$, we propose a numerical time discretization algorithm. For this, we consider a time interval $[t_n, t_{n+1}]$ for which we assume that $\bar{\boldsymbol{\varepsilon}}_n$ (macro strain at t_n), $\Delta\bar{\boldsymbol{\varepsilon}}$ (macro strain increment) and all history variables at t_n are known. The algorithm is described hereafter:

1. Initialization of the average strain increment in the inclusion phase:

   $\langle\Delta\boldsymbol{\varepsilon}\rangle_{w_1} = \Delta\bar{\boldsymbol{\varepsilon}}$

2. Take the regularized tangent operator $\hat{\mathbf{C}}_1^{\mathrm{reg}}$ as reference modulus (for this work, the behavior of inclusions is linear elastic, so, $\hat{\mathbf{C}}_1^{\mathrm{reg}} = \mathbf{C}_1^{\mathrm{el}}$) for the inclusions phase. $\langle\boldsymbol{\varepsilon}_n\rangle_{w_1}$ and $\langle\Delta\boldsymbol{\varepsilon}\rangle_{w_1}$ are introduced as input.
3. Compute average strain in matrix phase: $\langle\Delta\boldsymbol{\varepsilon}\rangle_{w_0} = \frac{1}{v_0}[\Delta\bar{\boldsymbol{\varepsilon}} - v_1\langle\Delta\boldsymbol{\varepsilon}\rangle_{w_1}]$

Please cite this article in press as: Miled, B., et al. Micromechanical modeling of coupled viscoelastic–viscoplastic composites based on an incrementally affine formulation. Int. J. Solids Struct. (2013), http://dx.doi.org/10.1016/j.ijsolstr.2013.02.004

4. Call VE–VP constitutive law of matrix material with $\langle \boldsymbol{\varepsilon}_n \rangle_{w_0}$ and $\langle \Delta\boldsymbol{\varepsilon} \rangle_{w_0}$ as an input. Compute the regularized tangent operator $\hat{\mathbf{C}}_0^{\text{reg}}$.
5. Extract isotropic part $\hat{\mathbf{C}}_0^{\text{iso}}$ from reference matrix modulus $\hat{\mathbf{C}}_0^{\text{reg}}$.
6. Compute Eshelby's tensor $\mathbf{S}$ (which is function of $\hat{\mathbf{C}}_0^{\text{iso}}$ and the shape of the inclusions) and the strain concentration tensor $\mathbf{B}$ (Eq. (B.6)) with this isotropic modulus.
7. Check compatibility of average strain in inclusions phase by computing the residual (computed from Eq. (B.3)):

$$\mathbf{R} = \mathbf{B} : [v_1\mathbf{B} + v_0\mathbf{I}]^{-1} : \Delta\bar{\boldsymbol{\varepsilon}} - \langle \Delta\boldsymbol{\varepsilon} \rangle_{w_1} + \mathbf{a}^{\epsilon}$$

where $\mathbf{a}^{\epsilon}$ is expressed in Eq. (B.4).
8. If $|\mathbf{R}|$ <Tolerance, then exit the loop,
9. else: new iteration (go to step 2) with new $\langle \Delta\boldsymbol{\varepsilon} \rangle_{w_1}$:

$$\langle \Delta\boldsymbol{\varepsilon} \rangle_{w_1} \leftarrow \langle \Delta\boldsymbol{\varepsilon} \rangle_{w_1} + \xi\mathbf{R}; \xi \in]0, 1].$$

For all numerical simulations, we used a value of $\xi = 1$.
10. After convergence, compute macro tangent operator:

$$\bar{\mathbf{C}} = [v_0\hat{\mathbf{C}}_0^{\text{iso}} + v_1\mathbf{C}_1^{\text{el}} : \mathbf{B}] : [v_0\mathbf{I} + v_1\mathbf{B}]^{-1}$$

Finally, compute macro stress increment (Eq. (48)).

5. Results and discussion

In order to assess the semi-analytical MFH method, we have carried out finite element (FE) simulations of a continuous VE–VP matrix reinforced by ellipsoidal or spherical inclusions with linear elastic behavior. For this, the proposed algorithms for the VE–VP model were implemented in the ABAQUS, 2009 FE software via a user defined material routine (UMAT). At each time step, each iteration of the FE equilibrium equations, and each integration point, the total strain increment and the history variables at the beginning of the step are passed to the UMAT, which must in turn compute the Cauchy stress and the algorithmic tangent matrix. For each FE analysis, the composite's macroscopic stress equals the volume average of the stress over the unit cell, which is computed as follows:

$$\bar{\boldsymbol{\sigma}} = \frac{1}{V}\sum_{k=1}^{N_k} \boldsymbol{\sigma}_k V_k \tag{56}$$

where $\boldsymbol{\sigma}_k$ is the stress acting at integration point k, V_k is the volume attached to integration point k, and N_k is the number of integration points within the volume V. As an example, we consider a composite material made of a polycarbonate polymer matrix reinforced with glass particles or fibers. The elastic properties of the particles are $E_1 = 76$ GPa and $v_1 = 0.22$, and those of the matrix are collected in Table 1 which presents parameters of polycarbonate at 22 °C based on experimental data collected from Frank (1997). The parameters were identified based on measured data from uniaxial compression tests. The hardening matrix's function considered in the following is of power-law type:

$$R(p) = kp^n \tag{57}$$

where k [MPa] is the hardening modulus and n the hardening exponent. The matrix's overstress due to the rate-dependence also obeys a power-law (see Eq. (24)). In this work, different unit cells were considered: 2D axisymmetric unit cell model and a 3D one. All MF simulations presented in this section took a few seconds of CPU time on an ordinary PC. On the contrary, the FE simulations took several minutes with 2D axisymmetric unit cell, and more than 24 h of CPU time with 3D unit cell.

Table 1
Constitutive model parameters for polycarbonate at 22 °C.

Viscoelastic parameters			
Initial shear modulus	G_0=1074 MPa		
Initial bulk modulus	K_0=3222 MPa		
G_i(MPa)	g_i(s)	K_j(MPa)	k_j(s)
157	0.0021	472	0.007
80	0.00378	242	0.126
37	0.0248	111	0.216
viscoplastic parameters			
Hardening function	k = 150 MPa	n = 0.43	
Viscoplastic function	κ=150 s^{-1}	m = 5	
Yield stress	σ_y=35 MPa		

5.1. 2D axisymmetric unit cell

The volume fraction of particles is 15%. Assuming a periodic microstructure and uniaxial stress tests, a 2D axisymmetric unit cell is defined and depicted in Fig. 1(a). The prescribed boundary conditions are the following. Zero displacements are imposed in the radial direction on the left vertical side and in the vertical direction on the bottom horizontal side. The right vertical side is constrained to have uniform radial displacement. Uniform vertical displacement is imposed on the top horizontal side.

We used the GMSH (Geuzaine and Remacle, 2009) software to mesh the geometry, and a typical mesh comprises approximately 1000 elements and 2700 nodes. A comparison of the predictions to those obtained with finer meshes is performed in order to study the convergence. Finally, the FE computations are conducted using ABAQUS software using six-noded triangular elements (CAX6) for the inclusion phase and eight-noded quadratic elements (CAX8) for the matrix phase.

The influence of time step size is illustrated in Fig. 2. For this, we present the predictions of tension test at the strain rate of 10^{-3} s^{-1} with different numbers of time steps, and we apply special isotropisation method to algorithmic and regularized tangent operators. In the latter case, it is shown that the result is independent of the number of time steps and the best prediction compared to the FE simulation is obtained also.

The numerical simulations of the effective response for a complete loading cycle are plotted in Figs. 3–5. Curves for three different strain rates 0.005 (Fig. 3), 0.5 (Fig. 4) and 6 s^{-1} (Fig. 5) are included, and comparison between FE simulations and predictions of MFH method (the proposed incrementally affine theory) is made. The figures show that MF predictions during different loading stages are comparable to FE ones, and that the MF results are too stiff for all strain rates. We remark also that the accuracy of the predictions decreases systematically as the strain rate decreases.

In order to identify the origin of the discrepancy between MFH and FE predictions, we performed simulations of composites with VE matrix (Fig. 6) and EVP matrix (Fig. 7). The behavior of the VE matrix is obtained taking material parameters of Table 1 with $\sigma_y \to \infty$. The behavior of the EVP matrix is obtained taking material parameters of Table 1 with $g_i \to \infty$ and $k_j \to \infty$. The loss of accuracy at small strain rates may be attributed mostly to the viscoelastic part of the response (Fig. 6). On the other hand, MFH predictions for a EVP matrix remain satisfying even at small strain rates.

Stress relaxation results are presented in Fig. 8. During the first stage of the uniaxial tension test, the sample is loaded at a constant strain rate of 6 s^{-1}, and after time $t = 0.0083$ s the strain is held constant, leading to stress relaxation.

The impact of the parameter (m) of the viscoplastic function on the stress–strain relationship of the composite is illustrated in

Please cite this article in press as: Miled, B., et al. Micromechanical modeling of coupled viscoelastic–viscoplastic composites based on an incrementally affine formulation. Int. J. Solids Struct. (2013), http://dx.doi.org/10.1016/j.ijsolstr.2013.02.004

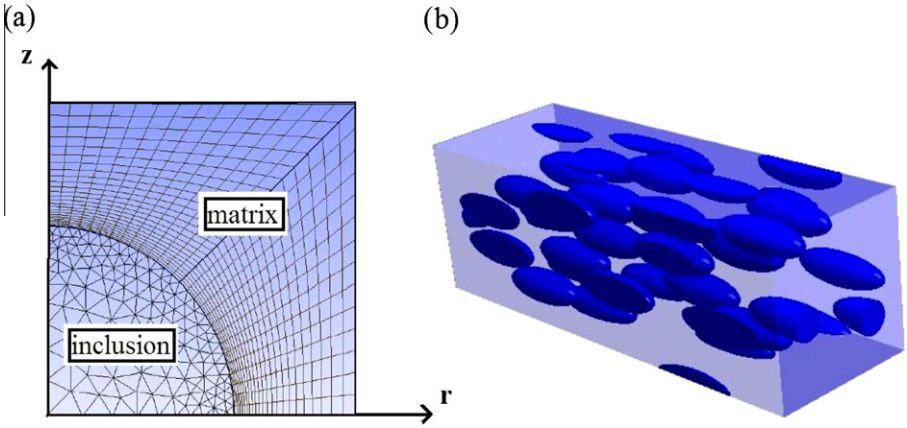

Fig. 1. (a) 2D Unit cell representation of a two-phase composite with periodic microstructure under axisymmetric loading, (b) Representative volume element (RVE) countaining ellipsoidal inclusions.

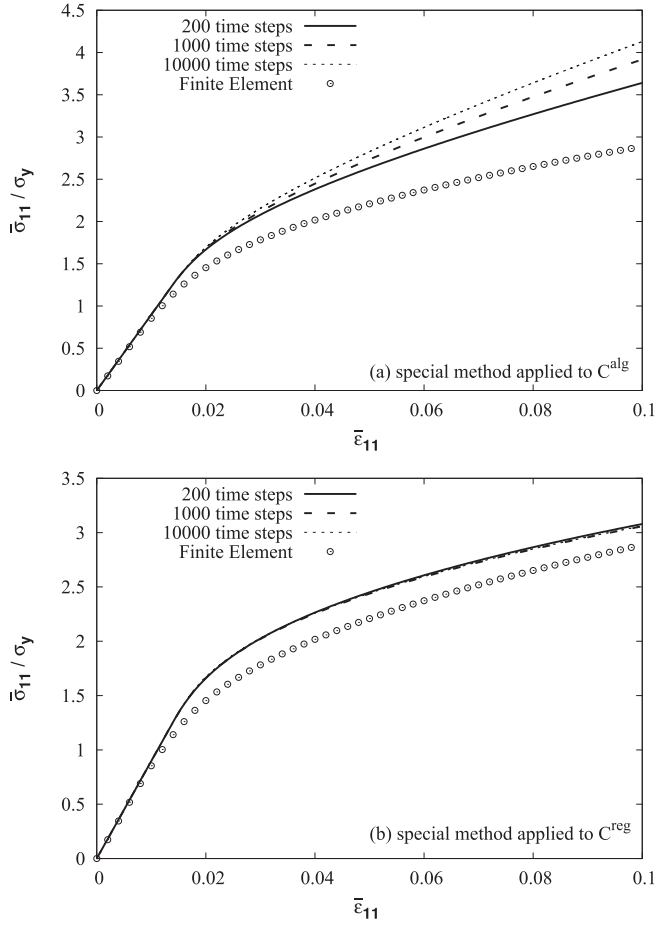

Fig. 2. tension test at the strain rate of 10^{-3} s^{-1} for a volume fraction of spherical inclusions equal to 15% with different numbers of time steps (200, 1000 and 10000), and using special isotropisation method. The FE simulations are shown for comparison. Data from Table 1.

Fig. 9. Three values of matrix viscoplastic exponent are considered: $m = 1, 5$ and 20. This figure shows that the MF response is stiffer than the FE result and that the discrepancy worsens with increasing m value. At the microscale, when $m \geqslant 1$, it follows from Eqs. (7), (11) and (24) that:

$$\sigma_{eq} = (\sigma_y + R(p))\left[1 + \left(\frac{\dot{p}}{\kappa}\right)^{1/m}\right] > \sigma_y + R(p)$$

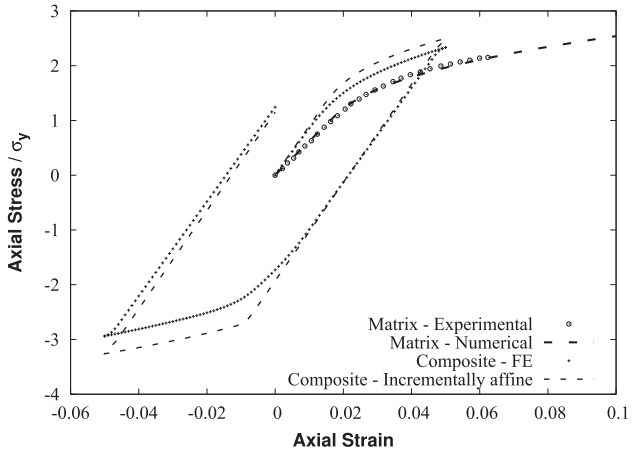

Fig. 3. Polycarbonate matrix reinforced with elastic spherical particles. Uniaxial cyclic loading at the strain rate of 0.005 s^{-1} for a volume fraction of inclusions equal to 15%. Comparison between FE simulations and predictions of the proposed incrementally affine theory. Fitted matrix material parameters are listed in Table 1.

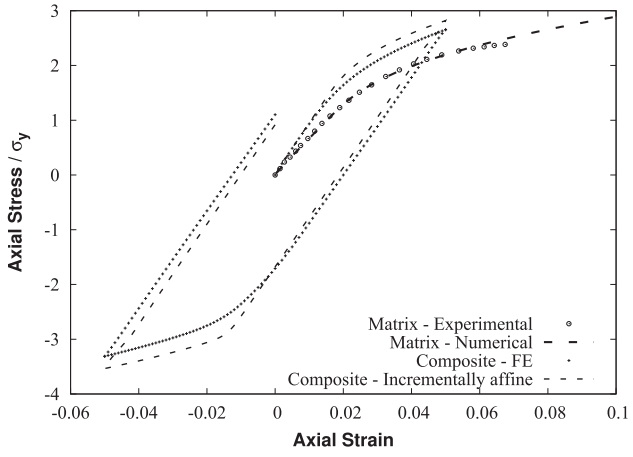

Fig. 4. Polycarbonate matrix reinforced with elastic spherical particles. Uniaxial cyclic loading at the strain rate of 0.5 s^{-1} for a volume fraction of inclusions equal to 15%. Comparison between FE simulations and predictions of the proposed incrementally affine theory. Fitted matrix material parameters are listed in Table 1.

Please cite this article in press as: Miled, B., et al. Micromechanical modeling of coupled viscoelastic–viscoplastic composites based on an incrementally affine formulation. Int. J. Solids Struct. (2013), http://dx.doi.org/10.1016/j.ijsolstr.2013.02.004

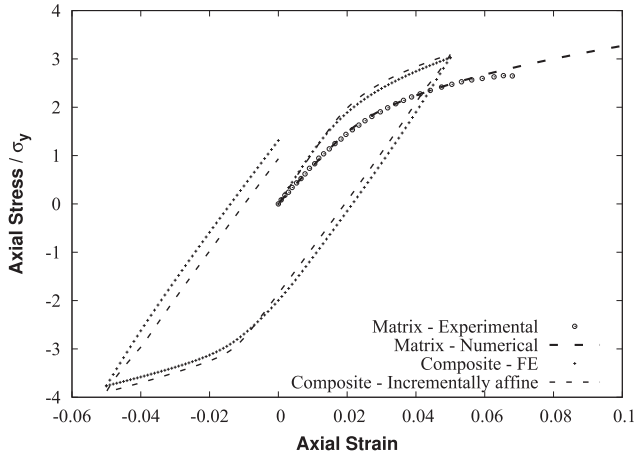

Fig. 5. Polycarbonate matrix reinforced with elastic spherical particles. Uniaxial cyclic loading at the strain rate of 6 s^{-1} for a volume fraction of inclusions equal to 15%. Comparison between FE simulations and predictions of the proposed incrementally affine theory. Fitted matrix material parameters are listed in Table 1.

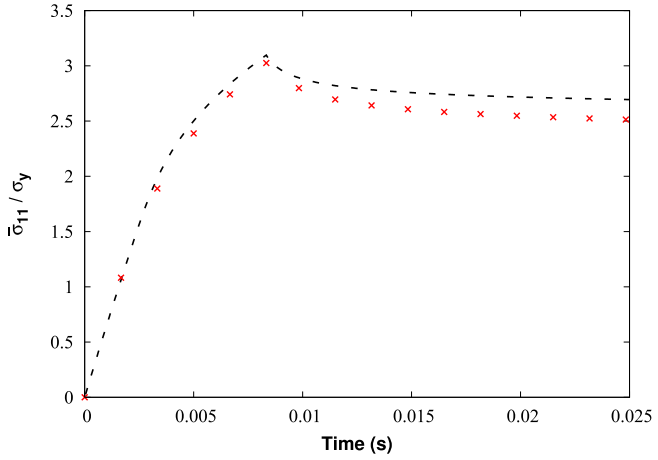

Fig. 8. Finite-element (symbols) and incrementally affine homogenization (dashed line) results for a volume fraction of inclusions of 15%. Two-stage uniaxial load: (1) strain rate of 6 s^{-1} up to time $t = 0.00833$ s, (2) relaxation. Fitted matrix material parameters are listed in Table 1.

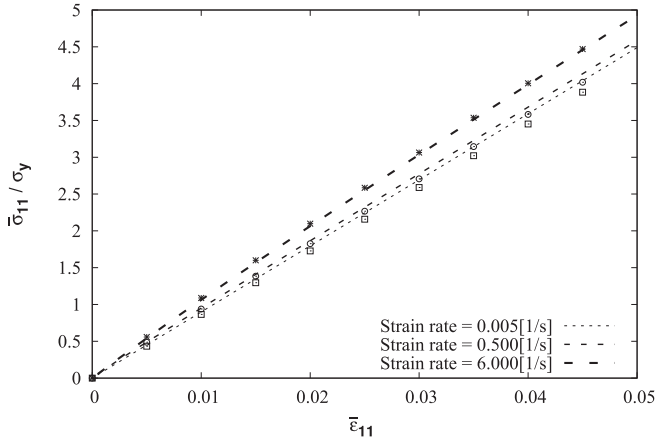

Fig. 6. Viscoelastic matrix reinforced with elastic spherical particles. Finite-element (symbols) and incrementally affine homogenization (solid lines) results for uniaxial tension at different strain rates for a volume fraction of inclusions equal to 15%.

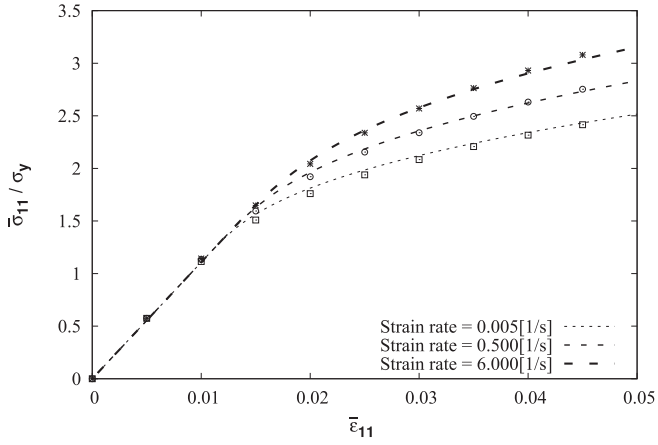

Fig. 7. Elasto-viscoplastic matrix reinforced with elastic spherical particles. Finite-element (symbols) and incrementally affine homogenization (solid lines) results for uniaxial tension at different strain rates for a volume fraction of inclusions equal to 15%.

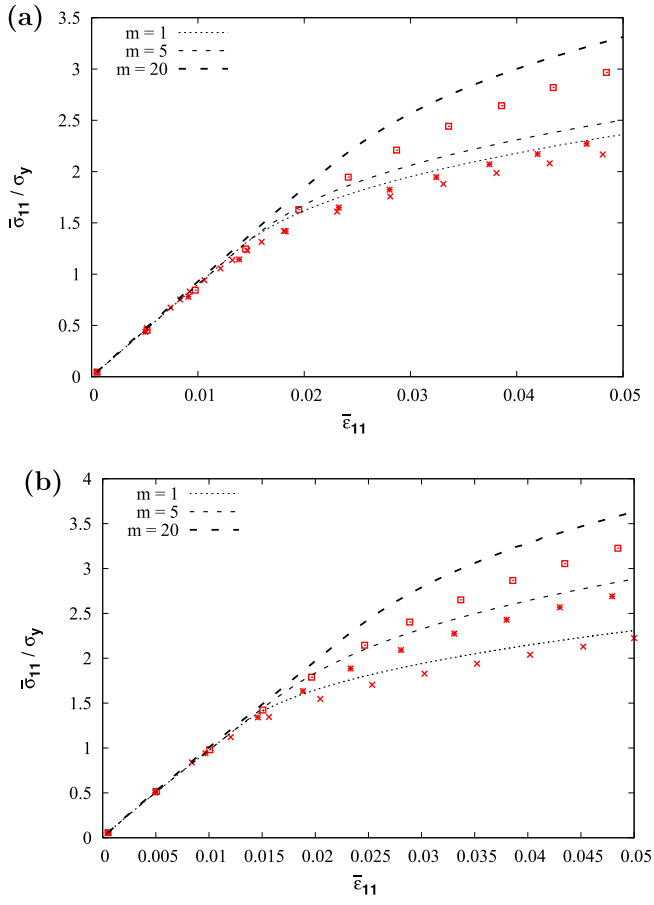

Fig. 9. Finite-element (symbols) and incrementally affine homogenization (dashed line) results for uniaxial tension test for a volume fraction of inclusions of 15%, for different viscoplastic exponents (m) with two strain rates: (a) 0.005 s^{-1}, (b) 1 s^{-1}. Fitted matrix material parameters are listed in Table 1.

Therefore, if $0 < \frac{\dot{p}}{\kappa} < 1$, the equivalent stress σ_{eq} increases if we increase the value of m. In terms of MF predictions, the resulting increase of σ_{eq} leads to a stiffer and less accurate prediction.

Please cite this article in press as: Miled, B., et al. Micromechanical modeling of coupled viscoelastic–viscoplastic composites based on an incrementally affine formulation. Int. J. Solids Struct. (2013), http://dx.doi.org/10.1016/j.ijsolstr.2013.02.004

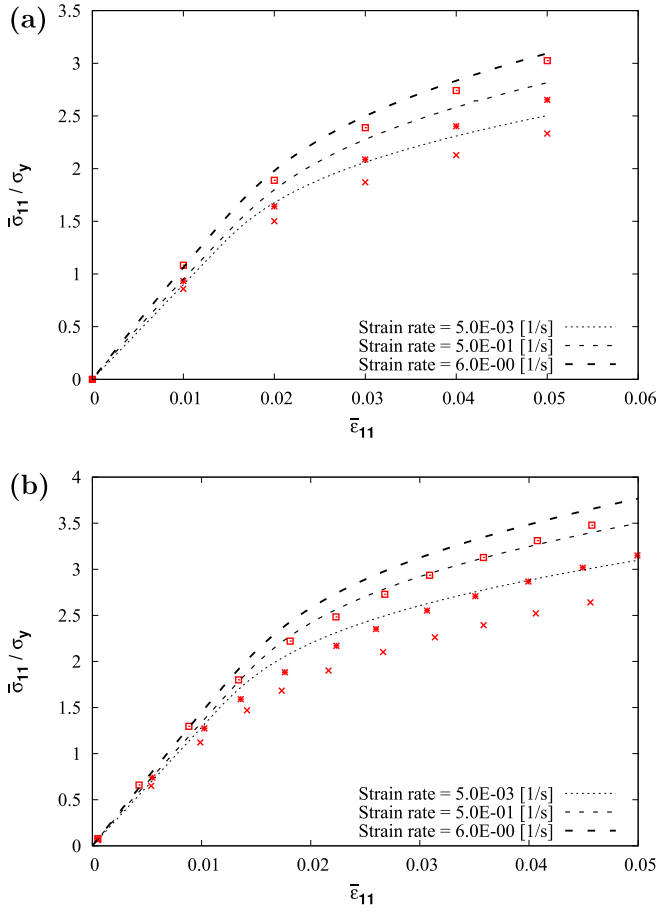

Fig. 10. Finite-element (symbols) and incrementally affine homogenization (dashed line) results for uniaxial tension test at different strain rates with two volume fractions of spherical inclusions: (a) 15%, (b) 30%. Fitted matrix material parameters are listed in Table 1.

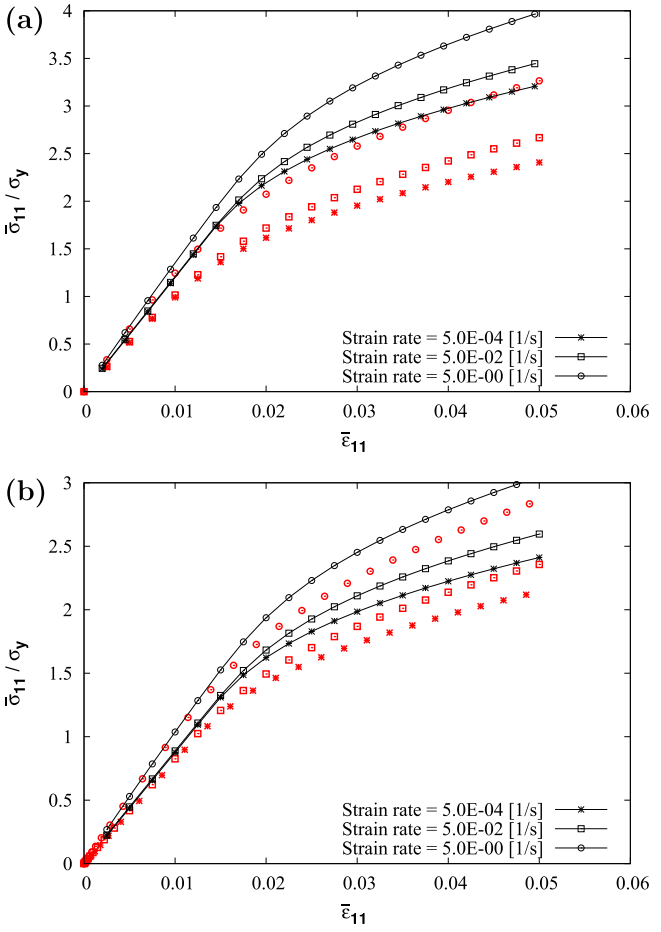

Fig. 11. Polycarbonate matrix reinforced with elastic ellipsoidal particles. Uniaxial tension loading at different strain rates for a volume fraction of inclusions equal to 15% and aspect ratio $\alpha = 3$. Comparison between finite-element (symbols) simulations and predictions of the proposed incrementally affine (solid lines with symbol) theory. Uniaxial tension is performed either in the direction of the inclusions axis (a) or tranversely to the inclusions axis (b). Fitted matrix material parameters are listed in Table 1.

The numerical simulations of the effective response in uniaxial tension for 15% and 30% volume fraction of inclusions at different strain rates are illustrated on Fig. 10. For decreasing strain rates, responses become softer and should tend to the rate independent one. The rate of loading has a significant effect on the mechanical response in both the viscoelastic and the viscoplastic regime. The two homogenization methods produce similar predictions. However, the proposed incrementally affine method tends to overestimate the stresses at composite level.

5.2. 3D representative cell

For the 3D representative cell, a parallelepipedic unit cell of size $(30 \times 10 \times 10)$ for inclusions aligned with their revolution axis is defined and depicted in Fig. 1(b). The microstructure is filled with 30 ellipsoidal inclusions and the mesh comprises about 2,00,000 second-order tetrahedra (C3D10M in ABAQUS). The fibers' volume fraction is $v_1 = 15\%$ and their aspect ratio $\alpha = 3$. For the aligned fibers microstructure, a uniaxial loading is applied either in the longitudinal or a transverse direction w.r.t. (with respect to) the inclusion revolution axis. We note that the generation of the random distribution follows Pierard et al. (2007b).

The predictions of the effective behavior provided by the MFH model and the FE results for a uniaxial loading applied either in the longitudinal or the transverse direction are presented in Fig. 11. It is observed that the MFH method overestimates the macroscopic stress whatever the direction of loading (longitudinal or transversal) and the strain-rate. When the loading is applied in the transverse direction w.r.t. the inclusion revolution axis, the discrepancy between FE simulations and predictions of the proposed incrementally affine theory (computed as $\frac{\bar{\sigma}^{MF}-\bar{\sigma}^{FE}}{\bar{\sigma}^{FE}}$) varies between 10% for $\dot{\varepsilon} = 0.0005\ s^{-1}$ and 7% for $\dot{\varepsilon} = 5\ s^{-1}$. The predictions are a lot less accurate when the loading is applied in the longitudinal direction w.r.t. the inclusion axis. The per phase average stresses are depicted for a matrix reinforced by 15% of ellipsoidal inclusions at the strain rate of $0.05\ s^{-1}$ in the longitudinal (Fig. 12(a)) and transverse (Fig. 12(b)) direction w.r.t. the inclusion axis. A good agreement is observed between results predicted by our MFH method and those obtained by FE simulations for the average stress in the matrix phase. However, the average stress in the inclusions is overestimated. This observation is more pronounced for a loading in the longitudinal direction. Fig. 13 presents contour plots of the accumulated plastic strain in the matrix for both loading directions. In the longitudinal case, deformation is concentrated at the ends of the elongated fibers, while other matrix regions present a relatively low and homogeneous level of plastic strain. When loading is applied transversely to the direction of the fibers, the plastic strain distribution is much more homogeneous, except for some zones very close to the particle/matrix interfaces. In addition, the plastic strain reaches locally much higher values in the longitudinal case than in the transverse one.

Please cite this article in press as: Miled, B., et al. Micromechanical modeling of coupled viscoelastic–viscoplastic composites based on an incrementally affine formulation. Int. J. Solids Struct. (2013), http://dx.doi.org/10.1016/j.ijsolstr.2013.02.004

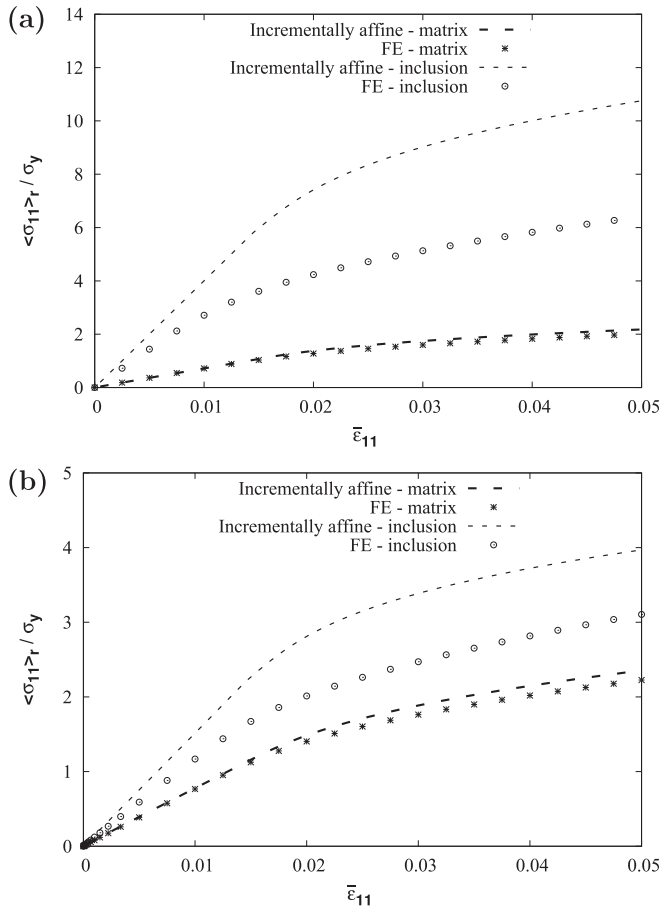

Fig. 12. Polycarbonate matrix with 15% of ellipsoidal elastic inclusions under uniaxial tension test at the strain rate of 0.05 s^{-1}: Mean-field homogenization (solid lines) and finite-element (symbols) predictions of average stresses in both phases. Uniaxial tension is performed either in the direction of the inclusions axis (a) or tranversely to the inclusions axis (b). Data from Table 1.

Similar observations were made for the MFH of elasto-plastic composites with ellipsoidal inclusions (see Doghri et al., 2010b, 2007b). All these observations show that the effects of stress concentrations are more crucial when loading is applied in the longitudinal direction w.r.t. the inclusion revoluion axis, and are less important when the composite is loaded in the transverse direction. These observations explain why for a loading in the fiber direction, the numerical predictions of the incrementally affine method based on first moments show a poor match against FE reference results.

5.3. Validation against experimental data

The numerical predictions were validated against experimental data (for unreinforced matrix material, and composite) reported by Drozdov et al. (2003). The material properties of the unreinforced polycarbonate matrix are collected in Table 1 except that $\sigma_y = 32$ MPa and $k = 120$ MPa. The composite is made of a polycarbonate matrix reinforced with 10% of short glass fibers with an aspect ratio of the order of 100 and subjected to uniaxial tension at the strain rate of 0.0011 s^{-1}. The elastic properties of the fibers are $E_1 = 76$ GPa and $\nu = 0.22$. With these data, Fig. 14 shows that we have a very good fit for the polycarbonate matrix. However, the prediction of the composite's response with incrementally affine formulation is too stiff.

5.4. Discussion

The *first part* of the MF simulations concern a VE–VP matrix reinforced with spherical inclusions, where the MF predictions were compared to FE simulations on unit cells, Figs. 2–10. In general, the MF results were found to be acceptable, and the regularized tangent operator of Eq. (27) provided time increment-independent predictions (Fig. (2)). However it was found that compared to FE simulations, the results worsen when decreasing the strain rate (e.g., Figs. 3–5) or increasing the VP function exponent m (e.g., Fig. (9)). Nevertheless, we cannot be conclusive about these observations. Firstly, such conclusions do not apply to EVP composites (see for instance Doghri et al. (2010a) and Brassart et al. (2012)). Secondly, the effect of the two parameters cannot be isolated of one another since the viscous stress (which is equal to the yield function f in the present formulation) depends on the strain rate. For instance, for the power law function of Eq. (24), we presume that the quality of predictions depends on the following dimensionless parameter (see Section 5.1): $(\dot{p}/\kappa)^{(1/m)}$. However, it is difficult to conduct an analytical study of MF accuracy because of the complexity of the effective stress expression (see (48)).

The quality of MF predictions also declines when increasing the volume fraction of the stiffer elastic spherical inclusions (Fig. (10)). This was also observed for other per-phase material models (e.g.,

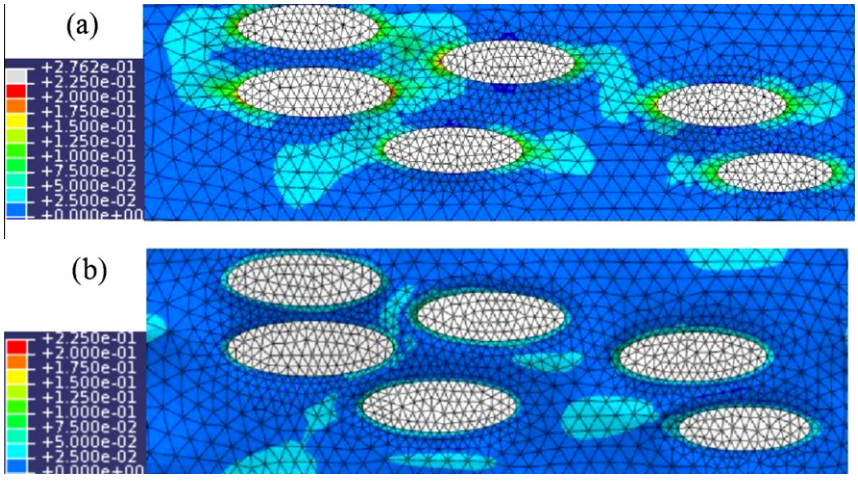

Fig. 13. Contour plot of the acumulated plastic strain in the matrix after tensile deformation up to 5% for a volume fraction of the ellipsoidal elastic inclusions equal to 15% and at the strain rate of 0.05 s^{-1}. The applied elongation is either in the direction of the fibers axis (a) or in the transverse direction (b).

Please cite this article in press as: Miled, B., et al. Micromechanical modeling of coupled viscoelastic–viscoplastic composites based on an incrementally affine formulation. Int. J. Solids Struct. (2013), http://dx.doi.org/10.1016/j.ijsolstr.2013.02.004

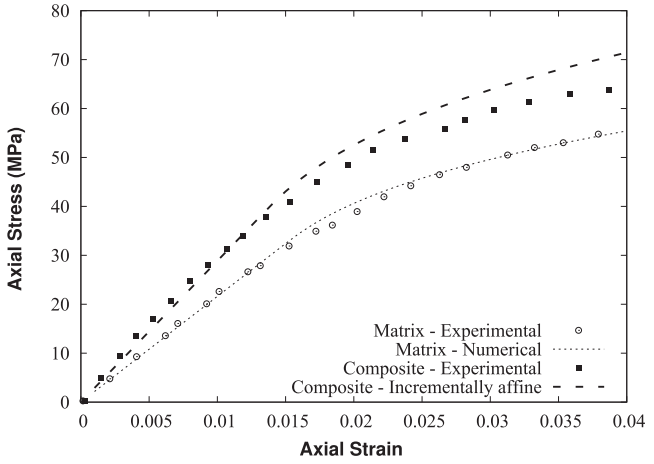

Fig. 14. Polycarbonate matrix reinforced with 10% of short glass fibers (with an aspect ratio of the order of 100) under uniaxial tension test at the strain rate of 0.0011 s^{-1}. Experimental data from Drozdov et al. (2003). Fitted matrix material parameters are listed in Table 1 (except that $\sigma_y = 32$ MPa and $k = 120$ MPa).

elasto-plastic or EVP) as can be seen in numerous papers listed in the bibliography section. Some of the inaccuracy is attributed to the Mori–Tanaka model itself which is used to homogenize the linear comparison composite (LCC). Indeed, it is known that this linear MF model becomes less accurate as the volume fraction of inclusions (v_1) increases. In addition, with increased v_1, the per-phase fields become more heterogeneous and a first-moment MF formulation (such as the one in the present work) has more difficulty to capture the heterogeneities with comparison materials based on simple per-phase volume averages of strain or stress microfields.

In the *second part* of the MF simulations, non-spherical elongated inclusions of an aspect ratio $\alpha = 3$ were embedded in a VE–VP matrix, and the MF predictions were verified against full-field FE simulations on RVEs (Figs. 11–13). The agreement with reference FE results was found to be much less satisfactory than for spherical inclusions (Fig. (11)). This can be explained by the inability of MF to predict the average response in the inclusions correctly (Fig. (12)), and by the heterogeneity of the plastic strain fields in the matrix (Fig. (13)) which is much more pronounced for elongated inclusions than for spherical ones. The trends here and the conclusions are similar to what was observed for other MF formulations for elasto-plastic (EP) or EVP materials reinforced with ellipsoidal inclusions, see for instance Pierard et al. (2007b), Doghri et al. (2010b) and Brassart et al. (2012). However, the VE–VP predictions are worse than with EP or EVP matrix materials, because for $\alpha = 3$, we should expect better results in the longitudinal direction, and the effective response in the transverse direction should even be "nailed down" by MF.

In the *third part* of the numerical study, a VE–VP matrix reinforced with glass fibers of an aspect ratio $\alpha = 100$ was simulated under uniaxial tension. The MF predictions compare relatively well with experimental data (Fig. (14)). This rather good agreement is unexpected, because the quality of first-moment MF predictions is known to decrease with increasing α, as can be seen for instance from the results published in Doghri et al. (2010b) for $\alpha = 15$ versus those of Pierard et al. (2007b) for $\alpha = 3$. Therefore, the quality of MF predictions for $\alpha = 100$ should be poorer than for $\alpha = 3$. The good match between MF and experimental results shown in Fig. (14) might be due to some MF approximations "canceling out". Indeed, experimentally, it is extremely difficult to manufacture a composite with aligned and equal-length glass fibers of an aspect ratio equal to 100, so MF is not actually modeling the real microstructure.

Examining all the verification results (Figs. 2–13), and although the MF predictions are generally acceptable and MF can also be inaccurate with other per-phase material models, it is observed that the MF predictions in VE–VP are worse than MF results in EVP. According to our investigations (some reported here and some not) the problem comes from the VE part of the response. Let us be more precise here. For a homogeneous VE–VP material, the numerical integration algorithm is accurate, as shown in Miled et al. (2011). For an EVP composite which can be retrieved from VE–VP by setting the per-phase VE relaxation times to infinity- the predictions of the incrementally affine MF formulation are acceptable and can even be quite accurate for spherical inclusions, as shown in Doghri et al. (2010b) and Brassart et al. (2012)– e.g. Figs. (10), (11) and (13) to (16) in the latter reference. However, in the present study it was found that the MF predictions in VE–VP are much less accurate than those of EVP, even for spherical inclusions. In our opinion, the problems comes from the comparison material of the VE part. Firsly, comparing Figs. (6) (pure VE matrix) and (7) (pure EVP matrix) gives a hint on the role played by the VE part on the inaccuracy of MF. Secondly, when the increment is purely VE (VP strains not evolving), the incrementally affine relation (37) becomes:

$$\Delta\boldsymbol{\sigma} = \widetilde{E} : (\Delta\boldsymbol{\epsilon} - \Delta\boldsymbol{\epsilon}^{\mathrm{af}}) \tag{58}$$

where the VE tangent operator $\widetilde{E}(\Delta t)$ is uniform per phase since it only depends on the time increment Δt. However the affine strain increment $\Delta\boldsymbol{\epsilon}^{\mathrm{af}}$ is given by Eq. (40) after setting $\Delta\boldsymbol{\epsilon}^{\mathrm{af}}_{\mathrm{evp}} = \mathbf{0}$. Therefore it is seen that $\Delta\boldsymbol{\epsilon}^{\mathrm{af}}$ is *not* uniform per phase since it depends on the per-phase viscous stresses at t_n. So the issue of comparison materials arises for the incrementally affine MF homogenization of VE–VP composites even if the increment is purely VE. This problem does *not* exist in EVP, where the per-phase elastic stiffness is homogeneous if the VP strains do not evolve. In our opinion, the issue of comparison material for the VE part of the response is the main reason behind the bad predictions of MF in VE–VP, as compared to MF in EVP. In addition to -or linked with- the comparison materials issue is the fact that in VE–VP, there are different relaxation times associated with both the VE and VP parts, while in EVP only VP relaxation times are present. Improving the MF treatment of the VE part of VE–VP is a difficult task. An idea is presented in Section 6.

6. Conclusions

A mean-field homogenization (MFH) scheme was proposed for inclusion-reinforced viscoelastic–viscoplastic (VE–VP) composites. A general incrementally affine linearization method was developed based on the local VE–VP model and the corresponding numerical algorithms which have been proposed recently by Miled et al. (2011). The affine formulation which has been developed by Doghri et al. (2010a) for EVP behavior was extended to VE–VP in this work. It provides an affine relation between stress and strain increments via an algorithmic tangent operator. Contrary to the original affine formulation, this method leads to thermoelastic-like relations directly in the time domain, and not in the Laplace–Carson (L–C) one. In order to find the incrementally affine expression, we start by the linearization of evolution equations of the VP strain $\boldsymbol{\epsilon}^{\mathrm{vp}}$ and the scalar and/or tensor internal variables $\mathbf{V}$ at time t_n around time t_{n+1}. Next, a numerical integration of the linearized equations is required using a fully implicit backward Euler scheme. The obtained algebraic equations lead to an incrementally affine formulation $\left(\Delta\boldsymbol{\sigma} = \mathbf{C}^{\mathrm{alg}}(t_{n+1}) : (\Delta\boldsymbol{\epsilon} - \Delta\boldsymbol{\epsilon}^{\mathrm{af}})\right)$ which is form-similar to linear thermoelasticity $\left(\boldsymbol{\sigma}(x) = \mathbf{C}^{\mathrm{el}} : (\boldsymbol{\epsilon}(x) - \boldsymbol{\epsilon}^{\mathrm{th}}(x))\right)$ for each VE–VP phase. In order to average the stress

Please cite this article in press as: Miled, B., et al. Micromechanical modeling of coupled viscoelastic–viscoplastic composites based on an incrementally affine formulation. Int. J. Solids Struct. (2013), http://dx.doi.org/10.1016/j.ijsolstr.2013.02.004

and strain fields over the two phases, a linear comparison composite (LCC) which is made of constituents (phases) that have uniform linearized mechanical properties varying only with time is considered. Known homogenization models for linear thermoelastic composites can then be applied.

Finite element (FE) analyses (2D axisymmetric and 3D unit cells) have been performed to verify the semi-analytical mean-field homogenization method. The MF results were presented in Sections 5.1, 5.2, 5.3, and discussed in Section 5.2. The predictions are generally acceptable, although they are much less satisfactory than those obtained for EVP composites with the incrementally affine linearization theory.

There are different ways to improve the proposed MF formulation. Within the first-moment homogenization framework, we could still use some key ingredients of the proposed formulation, namely the incrementally affine linearization, the regularized tangent operators and the special isotropisation technique. However, instead of homogenizing the linear comparison composite (LCC) with a simple analogy with linear thermoelasticity, we could instead extend the interaction law of Mercier and Molinari (2009) from EVP to coupled VE–VP. Indeed, the latter law which was shown to lead to good predictions in EVP is based on a separation between elastic and VP contributions. Similarly, its extended version would separate between VE and VP contributions, and therefore -hopefully- solve the problems due to the VE part in the present formulation.

Significant improvements of predictions can also be expected from a MF formulation based on second moments of per-phase stress or strain microfields. Indeed, second moments of the fields are related to their variance, therefore they represent a richer statistical information than the simple volume averages (first moments) and taking them into account can lead to much better predictions. The second moment enrichment of MF can be achieved either via a pragmatic approach, such as the second-moment incremental formulation proposed by Doghri et al. (2010b) for elasto-plastic composites, which could be extended to VE–VP via the incrementally affine linearization method. Another and more rigourous approach would be to develop a variational formulation for VE–VP composites, in the same spirit as the variational incremental formulation proposed by Brassart et al. (2012) for EVP.

Acknowledgements

Funding from Région Wallonne through the EUREKA DAMOFIP project (Rhodia Engineering Plastics, CEMEF-Ecole des Mines de Paris, e-Xstream engineering and UCL) is gratefully acknowledged. B. Miled gratefully acknowledges an assistantship from UCL. L. Brassart is mandated by the National Fund for Scientific Research (FNRS, Belgium).

Appendix A. Stress–Strain incremental relation via an algorithmic tangent operator

In Section 2.2, we showed that:

$$\Delta\boldsymbol{\sigma} = \widetilde{\mathbf{E}} : (\Delta\boldsymbol{\epsilon} - \Delta\boldsymbol{\epsilon}^{\mathrm{vp}}) + \mathbf{a}(t_n) \tag{A.1}$$

where $\mathbf{a}(t_n)$ is a second-order tensor:

$$\mathbf{a}(t_n) = -\sum_i \left[1 - \exp\left(-\frac{\Delta t}{g_i}\right)\right]\mathbf{s}_i(t_n) - \sum_j \left[1 - \exp\left(-\frac{\Delta t}{k_j}\right)\right]\sigma_{H_j}(t_n)\cdot\mathbf{1} \tag{A.2}$$

Replacing the expression of the VP strain increment (Eq. (34)) in Eq. (A.1), we find:

$$\Delta\boldsymbol{\sigma} = \widetilde{\mathbf{E}} : \left(\Delta\boldsymbol{\epsilon} - \left[\dot{\boldsymbol{\epsilon}}^{\mathrm{vp}}(t_n) + \tilde{\boldsymbol{\epsilon}}_{,\mathbf{V}}(t_{n+1}) \bullet [\ldots]^{-1} \bullet \dot{\mathbf{V}}(t_n) + \{\ldots\} : \Delta\boldsymbol{\sigma}\right]\Delta t\right) + \mathbf{a}(t_n) \tag{A.3}$$

$$\Rightarrow \left[\mathbf{I} + \widetilde{\mathbf{E}} : \{\ldots\}\Delta t\right] : \Delta$$

$$\boldsymbol{\sigma} = \widetilde{\mathbf{E}} : \left(\Delta\boldsymbol{\epsilon} - \underbrace{\left[\dot{\boldsymbol{\epsilon}}^{\mathrm{vp}}(t_n) + \tilde{\boldsymbol{\epsilon}}_{,\mathbf{V}}(t_{n+1}) \bullet [\ldots]^{-1} \bullet \dot{\mathbf{V}}(t_n)\right].\Delta t}_{\Delta\boldsymbol{\epsilon}^{\mathrm{af}}_{\mathrm{evp}}}\right) + \mathbf{a}(t_n) \tag{A.4}$$

$$\begin{aligned}\Rightarrow \Delta\boldsymbol{\sigma} &= \left[\mathbf{I} + \widetilde{\mathbf{E}} : \{\ldots\}\Delta t\right]^{-1} : \left[\widetilde{\mathbf{E}} : \left(\Delta\boldsymbol{\epsilon} - \Delta\boldsymbol{\epsilon}^{\mathrm{af}}_{\mathrm{evp}}\right) + \mathbf{a}(t_n)\right] \\ &= \mathbf{C}^{\mathrm{alg}} : \left(\Delta\boldsymbol{\epsilon} - \Delta\boldsymbol{\epsilon}^{\mathrm{af}}_{\mathrm{evp}} + \widetilde{\mathbf{E}}^{-1} : \mathbf{a}(t_n)\right) = \mathbf{C}^{\mathrm{alg}} : \left(\Delta\boldsymbol{\epsilon} - \Delta\boldsymbol{\epsilon}^{\mathrm{af}}\right)\end{aligned} \tag{A.5}$$

where $\mathbf{C}^{\mathrm{alg}}$ is the algorithmic tangent operator:

$$\mathbf{C}^{\mathrm{alg}} = \left[\widetilde{\mathbf{E}}^{-1} + \{\ldots\}\Delta t\right]^{-1} \tag{A.6}$$

and, $\Delta\boldsymbol{\epsilon}^{\mathrm{af}}$ is the affine strain increment in the viscoelastic–viscoplastic model:

$$\Delta\boldsymbol{\epsilon}^{\mathrm{af}} = \Delta\boldsymbol{\epsilon}^{\mathrm{af}}_{\mathrm{evp}} - \widetilde{\mathbf{E}}^{-1} : \mathbf{a}(t_n) \tag{A.7}$$

$\widetilde{\mathbf{E}}$ is an isotropic fourth-rank incremental relaxation modulus: $\widetilde{\mathbf{E}} = 2\widetilde{G}\mathbf{I}^{\mathrm{dev}} + 3\widetilde{K}\mathbf{I}^{\mathrm{vol}}$. So, the inverse of this modulus is given as follows:

$$\widetilde{\mathbf{E}}^{-1} = \frac{1}{2\widetilde{G}}\mathbf{I}^{\mathrm{dev}} + \frac{1}{3\widetilde{K}}\mathbf{I}^{\mathrm{vol}} \tag{A.8}$$

Combining Eqs. (A.2) and (A.8), and after some algebra, the VE–VP affine strain increment (Eq. (A.7)) becomes:

$$\begin{aligned}\Delta\boldsymbol{\epsilon}^{\mathrm{af}} = \Delta\boldsymbol{\epsilon}^{\mathrm{af}}_{\mathrm{evp}} &+ \frac{1}{2\widetilde{G}}\sum_i \left[1 - \exp\left(-\frac{\Delta t}{g_i}\right)\right]\mathbf{s}_i(t_n) \\ &+ \frac{1}{3\widetilde{K}}\sum_j \left[1 - \exp\left(-\frac{\Delta t}{k_j}\right)\right]\sigma_{H_j}(t_n).\mathbf{1}\end{aligned} \tag{A.9}$$

Appendix B. Mean field homogenization in thermo-elasticity

Consider a two-phase, linear thermo-elastic composite of local elastic stiffness $\mathbf{E}^{\mathrm{el}}(x)$ and thermal expansion $\boldsymbol{\alpha}(x)$. The composite is subjected to a macroscopic strain $\bar{\boldsymbol{\epsilon}}$ and to a uniform temperature change ΔT. At each point x of the composite, the local stress–strain relations are given by:

$$\begin{aligned}\boldsymbol{\sigma}(x) &= \mathbf{E}^{\mathrm{el}}(x) : (\boldsymbol{\epsilon}(x) - \boldsymbol{\epsilon}^{\mathrm{th}}(x)), \quad \boldsymbol{\epsilon}^{\mathrm{th}}(x) = \boldsymbol{\alpha}(x)\Delta T \\ &= \mathbf{E}^{\mathrm{el}}(x) : \boldsymbol{\epsilon}(x) + \boldsymbol{\beta}(x), \quad \boldsymbol{\beta}(x) = -\mathbf{E}^{\mathrm{el}}(x) : \boldsymbol{\alpha}(x)\Delta T\end{aligned} \tag{B.1}$$

We aim to determine the effective properties $\bar{\mathbf{C}}$ and $\bar{\boldsymbol{\beta}}$ of the thermo-elastic composite. Let us first consider any homogenization model defined in the isothermal case by its strain concentration tensors ($\mathbf{A}$ and $\mathbf{B}$):

$$\langle\boldsymbol{\epsilon}\rangle_{w_1} = \mathbf{B} : \langle\boldsymbol{\epsilon}\rangle_{w_0}, \quad \langle\boldsymbol{\epsilon}\rangle_{w_1} = \mathbf{A} : \langle\boldsymbol{\epsilon}\rangle_{w}$$

$$\mathbf{A} = \mathbf{B} : (v_1\mathbf{B} + v_0\mathbf{I})^{-1} \tag{B.2}$$

Next, a composite subjected to linear displacement boundary conditions corresponding to a macroscopic total strain $\bar{\boldsymbol{\epsilon}} = \langle\boldsymbol{\epsilon}\rangle$ and to a uniform temperature change ΔT is considered. The total strain average and the effective stress–strain relation read (see e.g. Lielens, 1999, 2004):

Please cite this article in press as: Miled, B., et al. Micromechanical modeling of coupled viscoelastic–viscoplastic composites based on an incrementally affine formulation. Int. J. Solids Struct. (2013), http://dx.doi.org/10.1016/j.ijsolstr.2013.02.004

$$\langle \boldsymbol{\epsilon} \rangle_{w_1} = \mathbf{A} : \bar{\boldsymbol{\epsilon}} + \mathbf{a}^{\epsilon}, \quad \langle \boldsymbol{\sigma} \rangle = \bar{\mathbf{C}} : \bar{\boldsymbol{\epsilon}} + \bar{\boldsymbol{\beta}} \tag{B.3}$$

where:

$$\begin{cases} \bar{\boldsymbol{\beta}} = v_0 \boldsymbol{\beta}_0 + v_1 \boldsymbol{\beta}_1 + v_1 \left(\mathbf{E}_1^{\mathrm{el}} - \mathbf{E}_0^{\mathrm{el}} \right) : \mathbf{a}^{\epsilon} \\ \mathbf{a}^{\epsilon} = (\mathbf{A} - \mathbf{I}) : \left(\mathbf{E}_1^{\mathrm{el}} - \mathbf{E}_0^{\mathrm{el}} \right)^{-1} : (\boldsymbol{\beta}_1 - \boldsymbol{\beta}_0) \end{cases} \tag{B.4}$$

where $\mathbf{a}^{\epsilon}$ is a second-order tensor and $\bar{\mathbf{C}}$ is the effective stiffness of the composite as computed in the isothermal case.

$$\bar{\mathbf{C}} = [v_0 \mathbf{E}_0^{\mathrm{el}} + v_1 \mathbf{E}_1^{\mathrm{el}} : \mathbf{B}] : [v_0 \mathbf{I} + v_1 \mathbf{B}]^{-1} \tag{B.5}$$

For instance, the strain concentration tensor of the Mori–Tanaka scheme is given by:

$$\mathbf{B} = [\mathbf{I} + \mathbf{P} : (\mathbf{E}_1^{\mathrm{el}} - \mathbf{E}_0^{\mathrm{el}})]^{-1} \tag{B.6}$$

where $\mathbf{P} = \mathbf{S} : (\mathbf{E}_0^{\mathrm{el}})^{-1}$ is Hill's polarization tensor and $\mathbf{S}$ is Eshelby's tensor, which depends only on the properties of the matrix and the inclusion shape.

Appendix C. Spectral isotropisation: isothermal VE–VP case

Consider a time interval $[t_n, t_{n+1}]$. In Section 3 (Incrementally affine linearisation method), we showed that the stress–strain relation is given as follows:

$$\Delta\boldsymbol{\sigma} = \mathbf{C}^{\mathrm{alg}}(t_{n+1}) : (\Delta\boldsymbol{\epsilon} - \Delta\boldsymbol{\epsilon}^{\mathrm{af}}) \tag{C.1}$$

In J_2 viscoplasticity, the algorithmic tangent operator at time t_{n+1} ($\mathbf{C}^{\mathrm{alg}}(t_{n+1})$) and the affine strain increment ($\Delta\boldsymbol{\epsilon}^{\mathrm{af}}$) are expressed as follows:

$$\mathbf{C}^{\mathrm{alg}} = \widetilde{\mathbf{E}} - \frac{\left(2\widetilde{G}\right)^2}{h_v} \mathbf{N} \otimes \mathbf{N} - \left(2\widetilde{G}\right)^2 \frac{\sigma_{eq} \Delta p}{\sigma_{eq} + 3\widetilde{G}\Delta p} \frac{\partial \mathbf{N}}{\partial \boldsymbol{\sigma}} - \frac{2\widetilde{G}}{h_v g_{,\sigma}} \mathbf{N} \otimes g_{,\epsilon}$$

$$\Delta\boldsymbol{\epsilon}^{\mathrm{af}} = \Delta\boldsymbol{\epsilon}_{\mathrm{evp}}^{\mathrm{af}} - \widetilde{\mathbf{E}}^{-1} : \mathbf{a}(t_n) = \Delta\boldsymbol{\epsilon}_{\mathrm{evp}}^{\mathrm{af}} + \frac{1}{2\widetilde{G}} \sum_i \left[1 - \exp\left(-\frac{\Delta t}{g_i} \right) \right] \mathbf{s}_i(t_n) + \frac{1}{3\widetilde{K}} \sum_j \left[1 - \exp\left(-\frac{\Delta t}{k_j} \right) \right] \sigma_{H_j}(t_n) \mathbf{1} \tag{C.2}$$

where $\Delta\boldsymbol{\epsilon}_{\mathrm{evp}}^{\mathrm{af}}$ is given by this expression:

$$\Delta\boldsymbol{\epsilon}_{\mathrm{evp}}^{\mathrm{af}} = \dot{p}(t_n) \Delta t \left[\mathbf{N}(t_n) + \mathbf{N}(t_{n+1}) \frac{g_{,p}(t_{n+1}) \Delta t}{1 - g_{,p}(t_{n+1}) \Delta t} \right] \tag{C.3}$$

We aim to compute the shear and bulk moduli by extending the spectral isotropisation method to $\mathbf{C}^{\mathrm{alg}}(t_{n+1})$ and the incrementally affine linearization. For this, we introduce the following hypotheses.

1. $\mathbf{N}_{n+1} = \mathbf{N}_n$ ($\Rightarrow \Delta\boldsymbol{\epsilon}_{\mathrm{evp}}^{\mathrm{af}} \,//\, \mathbf{N}$)
2. dev ($\Delta\boldsymbol{\epsilon}$) // $\mathbf{N}$, (true for $\Delta\boldsymbol{\epsilon}^{\mathrm{vp}}$, and a hypothesis for dev ($\Delta\boldsymbol{\epsilon}^{\mathrm{ve}}$))
3. dev ($\Delta\boldsymbol{\epsilon}^{\mathrm{af}}$) // $\mathbf{N}$ (true for $\Delta\boldsymbol{\epsilon}_{\mathrm{evp}}^{\mathrm{af}}$ if $\mathbf{N}_{n+1} = \mathbf{N}_n$, and an hypothesis for dev ($\widetilde{\mathbf{E}}^{-1} : \mathbf{a}(t_n)$))
4. the initial yield stress σ_y is constant ($\Rightarrow g_{,\epsilon} = \mathbf{0}$).

Using the previous hypotheses (especially 2 and 3), the deviatoric parts of the strain increment and the affine strain increment can be written as follows:

$$\mathrm{dev}(\Delta\boldsymbol{\epsilon}) \equiv \alpha\mathbf{N} \quad \mathrm{dev}(\Delta\boldsymbol{\epsilon})^{\mathrm{af}} \equiv \beta\mathbf{N}$$

we have:

$$(\mathbf{I}^{\mathrm{dev}} - \frac{2}{3}\mathbf{N} \otimes \mathbf{N}) : \mathbf{N} = \mathbf{0} \quad \text{because} \quad \mathbf{N} : \mathbf{N} = \frac{3}{2}$$

Using the two previous equations, the expression of the stress increment (Eq. (C.1)) can be rewritten as follows:

$$\begin{aligned} \Delta\boldsymbol{\sigma} &= \mathbf{C}^{\mathrm{alg}}(t_{n+1}) : \left(\alpha\mathbf{N} + \frac{1}{3}\mathrm{tr}(\Delta\boldsymbol{\epsilon})\mathbf{1} - \beta\mathbf{N} - \frac{1}{3}\mathrm{tr}(\Delta\boldsymbol{\epsilon}^{\mathrm{af}})\mathbf{1} \right) \\ &= (\alpha - \beta) \left[\mathbf{C}^{\mathrm{alg}}(t_{n+1}) + \gamma(\mathbf{I}^{\mathrm{dev}} - \frac{2}{3}\mathbf{N} \otimes \mathbf{N}) \right] \\ &\quad : \mathbf{N} + \widetilde{\mathbf{E}} : \frac{1}{3}\left(\mathrm{tr}(\Delta\boldsymbol{\epsilon}) - \mathrm{tr}(\Delta\boldsymbol{\epsilon}^{\mathrm{af}})\right)\mathbf{1} \end{aligned} \tag{C.4}$$

The objective, is to find γ such that:

$$\mathbf{C}^{\mathrm{alg}}(t_{n+1}) + \gamma(\mathbf{I}^{\mathrm{dev}} - \frac{2}{3}\mathbf{N} \otimes \mathbf{N}) = \mathbf{C}^{\mathrm{iso}}(t_{n+1}) \tag{C.5}$$

We have:

$$\widetilde{\mathbf{E}} = 2\widetilde{G}\mathbf{I}^{\mathrm{dev}} + 3\widetilde{K}\mathbf{I}^{\mathrm{vol}}, \quad \frac{\partial \mathbf{N}}{\partial \boldsymbol{\sigma}} = \frac{3}{2\sigma_{\mathrm{eq}}}(\mathbf{I}^{\mathrm{dev}} - \frac{2}{3}\mathbf{N} \otimes \mathbf{N}) \tag{C.6}$$

Using the last equation, and replacing $\mathbf{C}^{\mathrm{alg}}(t_{n+1})$ by its expression, Eq. (C.5) becomes:

$$\mathbf{C}^{\mathrm{iso}}(t_{n+1}) = \left(2\widetilde{G} - \left(2\widetilde{G}\right)^2 \frac{\Delta p}{\sigma_{eq} + 3\widetilde{G}\Delta p} \frac{3}{2} + \gamma \right) \mathbf{I}^{\mathrm{dev}} + 3\widetilde{K}\mathbf{I}^{\mathrm{vol}} \underbrace{- \left(\frac{\left(2\widetilde{G}\right)^2}{h_v} - \left(2\widetilde{G}\right)^2 \frac{\Delta p}{\sigma_{eq} + 3\widetilde{G}\Delta p} + \frac{2}{3}\gamma \right)}_{(1')} \mathbf{N} \otimes \mathbf{N} \tag{C.7}$$

We know that the fourth-order isotropic projection is written as follows:

$$\mathbf{C}^{\mathrm{iso}} = 2\mu_t \mathbf{I}^{\mathrm{dev}} + 3k_t \mathbf{I}^{\mathrm{vol}} \tag{C.8}$$

where μ_t and k_t are the tangent shear and bulk moduli, respectively. In order to respect the form of the previous equation, a condition is required for Eq. (C.7):

$$(1') = 0 \Rightarrow \gamma = \frac{3}{2}\left(2\widetilde{G}\right)^2 \left[-\frac{1}{h_v} + \frac{\Delta p}{\sigma_{eq} + 3\widetilde{G}\Delta p} \right] \tag{C.9}$$

Comparing Eqs. (C.7) and (C.8), and using the previous equation, the two scalars k_t and μ_t of isotropic stiffness tensor are given as follows:

$$3k_t = 3\widetilde{K}, \quad 2\mu_t = 2\widetilde{G}\left[1 - \frac{3\widetilde{G}}{h_v} \right] \equiv 2k_3 \tag{C.10}$$

References

ABAQUS, 2009. General-purpose finite element software. ABAQUS Inc., Pawtucket, RI, USA.

Aboudi, J., 2005. Micromechanically established constitutive equations for multiphase materials with viscoelasticviscoplastic phases. Mech. Time-Depend. Mater. 9, 121–145.

Berbenni, S., Favier, V., Lemoine, X., Berveiller, M., 2004. Micromechanical modeling of the elastic-viscoplastic behavior of polycrystalline steels having different microstructures. Mater. Sci. Eng. A 372, 128–136.

Berveiller, M., Zaoui, A., 1979. An extension of the self-consistent scheme to plastically-flowing polycrystals. J. Mech. Phys. Solids 26, 325–344.

Boltzmann, L., 1878. Wield. Ann. 5, 430.

Brassart, L., Stainier, L., Doghri, I., Delannay, L., 2012. Homogenization of elasto–(visco)plastic composites based on an incremental variational principle. Int. J. Plast. 36, 86–112.

Camacho, C.W., Tucker III, C.L., Yalvac, S., McGee, R.L., 1990. Stiffness and thermal expansion predictions for hybrid short fiber composites. Polym. Compos. 11, 229–239.

Chaboche, J.L., Kruch, S., Maire, J.F., Pottier, T., 2001. Towards a micromechanics based inelastic and damage modeling of composites. Int. J. Plast. 17, 411–439.

Doghri, I., 2000. Mechanics of Deformable Solids. Linear, Nonlinear, Analytical and Computational Aspects. Springer, Berlin.

Please cite this article in press as: Miled, B., et al. Micromechanical modeling of coupled viscoelastic–viscoplastic composites based on an incrementally affine formulation. Int. J. Solids Struct. (2013), http://dx.doi.org/10.1016/j.ijsolstr.2013.02.004

Doghri, I., Adam, L., Bilger, N., 2010a. Mean-field homogenization of elasto-viscoplastic composites based on a general incrementally affine linearization method. Int. J. Plast. 26, 219–238.

Doghri, I., Brassart, L., Adam, L., Gérard, J.D., 2010b. A second-moment incremental formulation for the mean-field homogenization of elasto-plastic composites. Int. J. Plast. 27, 352–371.

Drozdov, A.D., Al-Mulla, A., Gupta, R.K., 2003. The viscoelastic and viscoplastic behavior of polymer composites: polycarbonate reinforced with short glass fibers. Comput. Mater. Sci. 28, 16–30.

Dvorak, G., 1992. Transformation field analysis of inelastic composite materials. Proc. R. Soc. Lond. A 437, 311–327.

Eshelby, J.D., 1957. The determination of the elastic field of an ellipsoid inclusion, and related problems. Proc. R. Soc. Lond. A 241, 376–396.

Frank, G.J., 1997. Analytic and experimental evaluation of the effects of temperature and strain rate on the mechanical response of polymers. Report UDR-TR-97-152, University of Dayton Research Institute, Dayton, Ohio.

Frank, J.F., Brockman, R.A., 2001. A viscoelastic–viscoplastic constitutive model for glassy polymers. Int. J. Solids Struct. 38, 5149–5164.

Friebel, C., Doghri, I., Legat, V., 2006. General mean-field homogenization schemes for viscoelastic composites containing multiple phases of coated inclusions. Int. J. Solids Struct. 43, 2513–2541.

Geuzaine, C., Remacle, J.-F., 2009. Gmsh: a three-dimensional finite element mesh generator with built-in pre- and post-processing facilities. Int. J. Numer. Methods Eng. 79, 1309–1331.

Hashin, Z., 1965. Viscoelastic behavior of heterogeneous media. J. Appl. Mech. ASME 32E, 630–636.

Hashin, Z., 1970. Complex moduli of viscoelastic composites I. General theory and application to particulate composites. Int. J. Solids Struct. 6, 539–552.

Hershey, A.V., 1954. The elasticity of an isotropic aggregate of anisotropic cubic crystals. J. Appl. Mech. 21, 236–240.

Hill, R., 1965. A self-consistent mechanics of composite materials. J. Mech. Phys. Solids 13, 213–222.

Hill, R., 1965. Continuum micro-mechanics of elastoplastic polycrystals. J. Mech. Phys. Solids 13, 89101.

Hutchinson, J.W., 1976. Bounds and self-consistent estimates for creep of polycrystalline metals. Proc. R. Soc. Lond. A 348, 101–127.

Kim, J.S., Muliana, A.H., 2010. A combined viscoelastic–viscoplastic behavior of particle reinforced composites. Int. J. Solids Struct. 47, 580–594.

Kröner, E., 1958. Berechnung der elastischen Konstanten des Vielkristalls aus den Konstanten des Einkristalls. Z. Phys. 151, 504–518.

Kröner, E., 1961. Zur plastischen verformung des vielkristalls. Acta Metall. Mater. 9, 155–161.

Lahellec, N., Suquet, P., 2007a. Effective behavior of linear viscoelastic composites: a time-integration approach. Int. J. Solids Struct. 44, 507–529.

Lahellec, N., Suquet, P., 2007b. On the effective behavior of nonlinear inelastic composites: I: Incremental variational principles. J. Mech. Phys. Solids 55, 1932–1965.

Lahellec, N., Suquet, P., 2007c. On the effective behavior of nonlinear inelastic composites: II: A second-order procedure. J. Mech. Phys. Solids 55, 1964–1992.

Laws, N., McLaughlin, R., 1978. Self-consistent estimates for the viscoelastic creep compliances of composite materials. Proc. R. Soc. Lond. Ser. A 359, 251–273.

Lielens, G., 1999. Micromacro modeling of structured materials. Ph.D. Thesis, Université catholique de Louvain, Belgium.

Mareau, C., Favier, V., Berveiller, M., 2009. Micromechanical modeling coupling time-independent and time-dependent behaviors for heterogeneous materials. Int. J. Solids Struct. 46, 223–237.

Masson, R., Zaoui, A., 1999. Self-consistent estimates for the rate-dependent elasto-plastic behavior of polycrystalline materials. J. Mech. Phys. Solids 47, 1543–1568.

Masson, R., Bornert, M., Suquet, P., Zaoui, A., 2000. An affine formulation for the prediction of the effective properties of nonlinear composites and polycrystals. J. Mech. Phys. Solids 48, 1203–1227.

Mercier, S., Molinari, A., 2009. Homogenization of elastic-viscoplastic heterogeneous materials: Self-consistent and Mori–Tanaka schemes. Int. J. Plast. 25, 1024–1048.

Miled, B., Doghri, I., Delannay, L., 2011. Coupled viscoelastic–viscoplastic modeling of homogeneous and isotropic polymers: numerical algorithm and analytical solutions. Comput. Methods Appl. Mech. Eng. 200, 3381–3394.

Molinari, A., 2002. Averaging models for heterogeneous viscoplastic and elastic-viscoplastic materials. J. Eng. Mater. Technol. 124, 62–70.

Molinari, A., Canova, G.R., Ahzi, S., 1987. A self consistent approach at the large deformation polycrystal viscoplasticity. Acta Metall. 35, 2983–2994.

Molinari, A., Ahzi, S., Kouddane, R., 1997. On the self-consistent modeling of elastic–plastic behavior of polycrystals. Mech. Mater. 26, 43–62.

Mori, T., Tanaka, K., 1973. Average stress in matrix and average elastic energy of materials with misfitting inclusions. Acta Metall. 21, 571–574.

Muliana, A.H., Kim, J.S., 2007. A concurrent micromechanical model for nonlinear viscoelastic behaviors of particle reinforced composites. Int. J. Solids Struct. 44, 6891–6913.

Nemat-Nasser, S., Hori, M., 1999. Micromechanics: Overall Properties of Heterogeneous Materials, second ed. Elsevier, Amsterdam.

Nemat-Nasser, S., Obata, M., 1986. Rate-dependent, finite elasto-plastic deformation of polycrystals. Proc. R. Soc. Lond. A 407, 343–375.

Paquin, A., Sabar, H., Berveiller, M., 1999. Integral formulation and self-consistent modelling of elastoviscoplastic behavior of heterogeneous materials. Arch. Appl. Mech. 69, 14–35.

Pierard, O., 2006. Micromechanics of inclusion-reinforced composites in elasto-plasticity and elasto-viscoplasticity: modeling and computation. Ph.D. Thesis, Université catholique de Louvain, Belgium.

Pierard, O., Doghri, I., 2006a. An enhanced affine formulation and the corresponding numerical algorithms for the mean-field homogenization of elasto-viscoplastic composites. Int. J. Plast. 22, 131–157.

Pierard, O., Doghri, I., 2006b. Study of various estimates of the macroscopic tangent operator in the incremental homogenization of elasto-plastic composites. Int. J. Multiscale Comput. Eng. 4, 521–543.

Pierard, O., Friebel, C., Doghri, I., 2004. Mean-field homogenization of multi-phase thermo-elastic composites: a general framework and its validation. Compos. Sci. Technol. 64, 1587–1603.

Pierard, O., LLorca, J., Segurado, J., Doghri, I., 2007a. Micromechanics of particle-reinforced elasto-viscoplastic composites: finite element simulations versus affine homogenization. Int. J. Plast. 23, 1041–1060.

Pierard, O., Gonzalez, C., Segurado, J., LLorca, J., Doghri, I., 2007b. Micromechanics of elasto-plastic materials reinforced with ellipsoidal inclusions. Int. J. Solids Struct. 44, 6945–6962.

Ponte Castañeda, P., 1996. Exact second-order estimates for the effective mechanical properties of nonlinear composite materials. J. Mech. Phys. Solids 44, 827–862.

Sabar, H., Berveiller, M., Favier, V., Berbenni, S., 2002. A new class of micro-macro models for elastic-viscoplastic heterogeneous materials. Int. J. Solids Struct. 39, 3257–3276.

Simo, J.C., Hughes, T.J.R., 1998. Computational Inelasticity. Mechanics and Materials. Springer-Verlag New York Inc.

Tandon, G.P., Weng, G.J., 1988. A theory of particle-reinforced plasticity. J. Appl. Mech. 55, 126–135.

Weng, G.J., 1982. A unified self-consistent theory for the plastic-creep deformation of metals. J. Appl. Mech. 49, 728–734.

Please cite this article in press as: Miled, B., et al. Micromechanical modeling of coupled viscoelastic–viscoplastic composites based on an incrementally affine formulation. Int. J. Solids Struct. (2013), http://dx.doi.org/10.1016/j.ijsolstr.2013.02.004